AJRCCM Articles in Press. Published on 26-February-2018 as 10.1164/rccm.201709-1783OC

Protective Role of Myelocytic Nitric Oxide Synthases Against Hypoxic Pulmonary Hypertension in Mice

Takaaki Ogoshi[1], Masato Tsutsui[2], Takashi Kido[1], Mayuko Sakanashi[2], Keisuke Naito[1], Keishi Oda[1], Hiroshi Ishimoto[1,9], Sohsuke Yamada[3], Ke-Yong Wang[4], Yumiko Toyohira[5], Hiroto Izumi[6], Hiroaki Masuzaki[7], Hiroaki Shimokawa[8], Nobuyuki Yanagihara[5], Kazuhiro Yatera[1], Hiroshi Mukae[1,9]

Departments of [1]Respiratory Medicine, [3]Pathology, and [5]Pharmacology, School of Medicine, and [4]Shared-Use Research Center and [6]Department of Occupational Pneumology, Institute of Industrial Ecological Sciences, University of Occupational and Environmental Health, Kitakyushu, Japan; Departments of [2]Pharmacology and [7]Second Department of Internal Medicine, Graduate School of Medicine, University of the Ryukyus, Okinawa, Japan; [8]Department of Cardiovascular Medicine, Tohoku University Graduate School of Medicine, Sendai, Japan; and [9]Department of Respiratory Disease, Nagasaki University Graduate School of Biomedical Sciences, Nagasaki, Japan

Address for Correspondence:

Masato Tsutsui, MD, PhD, Professor and Chairman, Department of Pharmacology, Graduate School of Medicine, University of the Ryukyus, 207 Uehara, Nishihara, Okinawa 903-0215, Japan. Phone: +81-98-895-1133, Fax: +81-98-895-1411, E-mail: tsutsui@med.u-ryukyu.ac.jp

At a Glance Commentary:

Scientific Knowledge on the Subject: Nitric oxide (NO), synthesized by NO synthases (NOSs), plays a role in the development of pulmonary hypertension (PH). However, the role of NO/NOSs in bone marrow (BM) cells in PH remains to be clarified.

What This Study Adds to the Field: Here we show that transplantation of BM cells from mice lacking all NOSs aggravates hypoxia-induced PH in wild-type (WT) mice, and transplantation of BM cells from the WT mice ameliorates hypoxia-induced PH in the $NOSs^{-/-}$ mice, demonstrating a protective role of myelocytic NOSs in the pathogenesis of PH. Our findings provide novel insights into the cellular and molecular basis of PH.

(107 / 200 words)

Author contributions: T.O., M.T., T.K., K.Y., and H.M. designed research; T.O., T.K., M.S., H.I., S.Y., K-Y.W., Y.T., and H.I. performed research; T.O., M.T., T.K., H.Masuzaki., H.S., N.Y., K.Y., and H.Mukae. analyzed data; and T.O. and M.T. wrote the paper. All authors revised the paper, and approved the final version.

Sources of support: This work was supported in part by Grant-in-Aids for Young Scientists (B) (26860620) and Scientific Research (C) (16K09519) from the Japan Society for the Promotion of Science, a Grant for the UOEH Research Grant for Promotion of Occupational Health, and a Grant for the Promotion of Advanced Medicine from the Okinawa Prefecture, Japan.

A short running title: Protective role of myelocytic NO synthases in PH

Descriptor number: 17.06 Pulmonary hypertension, experimental

Total word count: 3,500 / 3,500 words with 7 figures, 9 supplementary figures, and 3 supplementary tables

This article has an online data supplement, which is accessible from this issue's table of contents online at www.atsjournals.org

AJRCCM Articles in Press. Published on 26-February-2018 as 10.1164/rccm.201709-1783OC

Abstract

Rationale: Nitric oxide (NO), synthesized by NO synthases (NOSs), plays a role in the development of pulmonary hypertension (PH). However, the role of NO/NOSs in bone marrow (BM) cells in PH remains elusive.

Objectives: To determine the role of NOSs in BM cells in PH.

Methods: Experiments were performed on 36 patients with idiopathic pulmonary fibrosis, and on wild-type (WT), neuronal (nNOS), inducible (iNOS), endothelial NOS (eNOS)$^{-/-}$, and n/i/eNOSs$^{-/-}$ mice.

Measurements and Main Results: In the patients, there was a significant correlation between higher pulmonary artery systolic pressure and lower NOx levels in the bronchoalveolar lavage fluid. In the mice, hypoxia-induced PH deteriorated significantly in the n/i/eNOSs$^{-/-}$ genotype and, to a lesser extent, in the eNOS$^{-/-}$ genotype as compared with the WT genotype. In the n/i/eNOSs$^{-/-}$ genotype exposed to hypoxia, the number of circulating BM-derived vascular smooth muscle progenitor cells was significantly larger, and transplantation of green fluorescent protein-transgenic BM cells revealed the contribution of BM cells to pulmonary vascular remodeling. Importantly, n/i/eNOSs$^{-/-}$-BM transplantation significantly aggravated hypoxia-induced PH in the WT genotype, and WT-BM transplantation significantly ameliorated hypoxia-induced PH in the n/i/eNOSs$^{-/-}$ genotype. 69 and 49 mRNAs related to immunity and inflammation, respectively, were significantly up-regulated in the lungs of WT genotype transplanted with n/i/eNOSs$^{-/-}$-BM compared with those with WT-BM, suggesting the involvement of immune and inflammatory mechanisms in the exacerbation of hypoxia-induced PH caused by n/i/eNOSs$^{-/-}$-BM transplantation.

Conclusions: These results demonstrate that myelocytic n/i/eNOSs play an important protective role in the pathogenesis of PH.

Keywords: bone marrow, pulmonary vascular remodeling, right ventricular hypertrophy, vascular smooth muscle progenitor cell

Introduction

Pulmonary hypertension (PH) is a progressive disease of the pulmonary microvasculature, leading to right ventricular failure and premature death. A recent large clinical study in a community-based general population of 10,314 subjects has reported that the prevalence of PH is 9.1% (1), indicating that PH is a common disease. Despite recent therapeutic advances, the prognosis for PH patients is still poor. In the ASPIRE registry, the 3-year survival rates for idiopathic PH (group 1), for PH due to left heart disease (group 2), for PH due to lung diseases and/or hypoxia (group 3), for chronic thromboembolic PH (group 4), and for miscellaneous PH (group 5) were 68%, 73%, 44%, 71%, and 59%, respectively (2). These survival rates are similar to or even worse than the 3-year survival rate for all cancers (69.5%) (3). Although several possible pathogenetic factors, including mutations in the bone morphogenic protein receptor 2 (BMPR2) gene, a deficiency in prostacyclin and nitric oxide (NO) release, and an excess in endothelin-1 and its receptor expression, have been thought to be involved in the development of PH (4), the precise mechanisms remain to be elucidated.

NO is synthesized from L-arginine by a family of NO synthases (neuronal [nNOS], inducible [iNOS], and endothelial NOS [eNOS]), all of which isoforms are expressed in human lung tissues under both physiological and pathological conditions (5-7). nNOS is located in the airway epithelium, vascular endothelium, vascular smooth muscle cells (VSMCs), and nerve cells; that iNOS is expressed in the airway epithelium, vascular endothelium, VSMCs, and alveolar macrophages; and that eNOS is localized in the vascular endothelium and VSMCs (8-10). There has been no previous study that characterizes the role of nNOS in PH. The detrimental role of iNOS in hypoxic PH has been reported by using an iNOS inhibitor (11), whereas the opposing protective role of iNOS has been shown in $iNOS^{-/-}$ mice (12). The beneficial role of eNOS in hypoxic PH has been indicated in $eNOS^{-/-}$ and eNOS-transgenic mice (13, 14), although conflicting results in the $eNOS^{-/-}$ mice have also been reported (15).

The role of the n/i/eNOSs in their entirety in PH has been examined in

AJRCCM Articles in Press. Published on 26-February-2018 as 10.1164/rccm.201709-1783OC

pharmacological studies with non-selective NOSs inhibitors, such as N^{ω}-nitro-L-arginine methyl ester (L-NAME). Although several studies have shown that the non-selective NOSs inhibitors potentiate pulmonary artery pressure (PAP) in animals with hypoxia-induced PH, there are also publications reporting a lack of such potentiations (16). It has been indicated that acute administration of L-NAME raised PAP in perfused lungs of rats with hypoxia-induced PH, but this effect was not reversed by administration of L-arginine, indicating that the effect of L-NAME was not mediated by NOSs inhibition (16). Thus, due to the non-specificity of non-selective NOSs inhibitors, the role of NOSs in the pathogenesis of PH still remains unclear. In this study, we addressed this issue in our mice lacking all NOSs (17). Recent studies have reported that myeloid abnormalities are associated with PH patients (18); that 13–48% of patients with bone marrow (BM) abnormalities (myeloproliferative disorders) suffer from PH (19); and that transplantation of BM cells with BMPR2 gene mutation causes PH in wild-type (WT) mice, suggesting the role of BM cells in the development of PH (20). However, no study has ever addressed the role of myelocytic NOSs in PH. Based on the aforementioned research, we investigated the role of NOSs, particularly myelocytic NOSs, in the development of PH. Some of the results of the study have been previously reported in the form of an abstract (21).

Methods

Subjects

This study was approved by the Institutional Review Board of the University of Occupational and Environmental Health. See Supplementary Methods for further details.

PASP Measured by Echocardiography

PASP was estimated by echocardiography (22, 23). See Supplementary Methods.

Animals

This study was approved by the Ethics Committee of Animal Care and Experimentation, the University of Occupational and Environmental Health. See Supplementary Methods.

Hypoxia Exposure

The mice were exposed to normoxia (21% O_2) or hypoxia (10% O_2) for 3 weeks. See Supplementary Methods.

Bronchoalveolar Lavage Fluid (BALF) Sampling

BALF sampling was performed as we previously reported (24). See Supplementary Methods.

NOx Measurement

NOx (nitrite plus nitrate) concentrations were assessed by the Griess method as we previously reported (17). See Supplementary Methods.

Western blot analysis

Western blot analysis was performed as we previously reported (25). See Supplementary Methods.

AJRCCM Articles in Press. Published on 26-February-2018 as 10.1164/rccm.201709-1783OC

Hemodynamics

Right ventricular systolic pressure (RVSP) was measured with a pressure transducer (Millar Instruments, Houston, TX) under anesthesia with sevoflurane. See Supplementary Methods.

Morphology

Haematoxylin-eosin or elastic-van Gieson (EVG) staining or α-smooth muscle actin (α-SMA) immunostaining was performed as we previously reported (26). See Supplementary Methods.

Treatment with Isosorbide Dinitrate (ISDN) or Sodium Nitrate

ISDN (0.6 mg/dl, Eisai, Tokyo, Japan) or sodium nitrate (2, 5, and 45 mmol/L, Wako, Osaka, Japan) was administered orally in the triple n/i/eNOS$^{-/-}$ mice from 3 days before to 3 weeks after the hypoxic exposure (27). See Supplementary Methods.

Bleomycin Treatment

Bleomycin (8.0 mg/kg/day, Nippon Kayaku, Tokyo, Japan) was intraperitoneally administered in the WT and triple n/i/eNOSs$^{-/-}$ mice for 10 consecutive days, and PH evaluation was performed at 14 days after the last administration (28). See Supplementary Methods.

BM-derived VSMC Progenitor Cells

After red blood cells were removed from anti-coagulated blood by erythrocyte lysis, stem cell antigen-1^{+} (Sca-1^{+})/c-kit^{-}/lineage^{-} (Lin^{-}) cells were counted with flow cytometry (Sony, Tokyo, Japan) as we previously reported (29). See Supplementary Methods.

Stromal Cell-Derived Factor (SDF)-1α

SDF-1α levels were measured with an immunoassay kit (R&D Systems, Minneapolis, MN). See Supplementary Methods.

BM Transplantation

BM transplantation was performed as we previously reported (30). See Supplementary Methods.

Fluorescent Staining

Immunofluorescence for α-SMA and 4',6-diamidino-2-phenylindole dihydrochloride (DAPI) was analyzed by confocal laser scanning microscopy. See Supplementary Methods.

Micro Computed Tomographic (CT) Analysis

A micro CT analysis was performed under sevoflurane anesthesia (RIGAKU, Tokyo, Japan). See Supplementary Methods.

RNA Sequencing

cDNA libraries were sequenced on an HiSeq 2500 platform (Illumina, San Diego, CA). See Supplementary Methods.

Statistical analyses

Results are expressed as mean ± SEM. Statistical analyses were performed by Student's *t*-test, or ANOVA followed by Bonferroni's test. See Supplementary Methods.

AJRCCM Articles in Press. Published on 26-February-2018 as 10.1164/rccm.201709-1783OC

Results

An Inverse Correlation Between PASP and NOx or Nitrate Levels in BALF in Patients with Idiopathic Pulmonary Fibrosis (IPF)

We performed detailed examinations, including bronchoscopy and Doppler echocardiography, in 303 subjects who were suspected to be suffering from interstitial lung diseases, in order to determine a diagnosis. We instructed current smokers to refrain from smoking for 2 weeks before the examinations in order to minimize the influence of smoking on the examinations. We did not measure a urinary or blood level of cotinine that is a metabolite of nicotine and a marker of current smoking status. We finally studied 36 consecutive patients with IPF. The baseline characteristics of the patients are shown in Supplementary Table E1. In the patients, PASP estimated by Doppler echocardiography was significantly and negatively correlated with BALF NOx levels and BALF nitrate levels, but not with BALF nitrite levels (Figure 1). There were no significant correlations between the BALF NOx, nitrate, or nitrite levels and BALF cellular profiles, lung function, serum lactate dehydrogenase or Krebs von den Lungen-6 levels, or partial pressure of oxygen in arterial blood (Supplementary Figure E1).

Lower Plasma and BALF NOx Levels in n/i/eNOSs$^{-/-}$ Mice Exposed to Hypoxia

We then conducted a basic study in which WT, single NOS$^{-/-}$, and triple n/i/eNOSs$^{-/-}$ mice were exposed to either normoxia or hypoxia for 3 weeks. After the normoxic exposure, the plasma NOx levels were significantly lower in the nNOS$^{-/-}$, iNOS$^{-/-}$, eNOS$^{-/-}$, and n/i/eNOSs$^{-/-}$ mice and lowest in the n/i/eNOSs$^{-/-}$ mice as compared with the WT mice (Figure 2A), and the BALF NOx levels were significantly reduced in the iNOS$^{-/-}$, eNOS$^{-/-}$, and n/i/eNOSs$^{-/-}$ mice and lowest in the n/i/eNOSs$^{-/-}$ mice (Figure 2B). As compared with the normoxic exposure, the hypoxic exposure did not significantly affect the plasma NOx levels in any of the mice (Figure 2A), but significantly increased the BALF NOx levels in the WT mice (Figure 2B). After both the normoxic and hypoxic exposure, the NOS$^{-/-}$ and n/i/eNOSs$^{-/-}$ mice were devoid of expression of genetically disrupted NOS and n/i/eNOSs, respectively (Figure 2C-F). As

compared with the normoxic exposure, the hypoxic exposure tended to increase expression levels of genetically intact NOSs in the lung in all the genotypes, and significantly up-regulated iNOS levels in the eNOS$^{-/-}$ mice and eNOS levels in the iNOS$^{-/-}$ mice (Figure 2C-F).

Up-regulation of arginase induces NO deficiency and NOS uncoupling via metabolizing L-arginine, and arginase expression is increased in the lung of patients with idiopathic PH (31). The hypoxic exposure significantly augmented arginase-1 levels in the lung in all the genotypes, and there were no significant differences in the hypoxia-induced arginase-1 levels among the five genotypes (Supplementary Figure E3).

Reduced Survival in n/i/eNOSs$^{-/-}$ Mice Exposed to Hypoxia

All the mice lived after the normoxic exposure, whereas after the hypoxic exposure, the survival rate was significantly worse in the n/i/eNOSs$^{-/-}$ mice and, to a lesser extent, in the eNOS$^{-/-}$ mice as compared with the WT mice (Figure 3A). After the hypoxic exposure, but not after the normoxic exposure, body weight was also significantly lower in the n/i/eNOSs$^{-/-}$ mice and, to a lesser degree, in the eNOS$^{-/-}$ mice compared with the WT mice (Supplementary Figure E2). A postmortem analysis indicated severe PH in all of the dead n/i/eNOSs$^{-/-}$ mice, and no other pathological findings that could explain the cause of death were observed in any of the mice (data not shown).

Accelerated Hypoxia-Induced PH in n/i/eNOSs$^{-/-}$ Mice

We next compared the extent of hypoxia-induced PH among the five genotypes. After the normoxic exposure, there were no significant differences in RVSP measured by right heart catheterization (an index of PASP), in the weight ratio of the right ventricle to the left ventricle plus the interventricular septum (RV/[LV+S]) (an index of RV hypertrophy [RVH]), or in the medial thickness of the small pulmonary arteries (an index of pulmonary vascular remodeling) in the five genotypes (Figures 3B-G). As compared with the normoxic exposure, the hypoxic exposure significantly increased the RVSP, RV/(LV+S), and medial thickness in all the five genotypes. Importantly, when the extents of these increases were

AJRCCM Articles in Press. Published on 26-February-2018 as 10.1164/rccm.201709-1783OC

compared among the five genotypes, the RVSP, RV/(LV+S), and medial thickness were all significantly accelerated in the n/i/eNOSs$^{-/-}$ mice and, to a lesser extent, in the eNOS$^{-/-}$ mice as compared with the WT mice (Figures 3B-G). Prominent muscularization of the media of the small pulmonary arteries was seen in the n/i/eNOSs$^{-/-}$ mice exposed to hypoxia (Figure 3F).

Since our original clinical question started with the IPF patients, we also used a bleomycin model that shows pulmonary fibrosis and PH. Bleomycin-induced increases in PH parameters were similarly more enhanced in the n/i/eNOSs$^{-/-}$ than in the WT mice (Supplementary Figure E6).

A NO Donor and Nitrate Reverse Hypoxia-Induced PH in n/i/eNOSs$^{-/-}$ Mice

We studied the effect of NO supplementation with ISDN or sodium nitrate on hypoxia-induced PH in the n/i/eNOSs$^{-/-}$ mice. Simultaneous oral treatment with ISDN or 5 mmol/L sodium nitrate significantly restored low plasma NOx levels, and improved reduced survival, weight loss, and increases in the RVSP, RV/(LV+S), and medial thickness in the n/i/eNOSs$^{-/-}$ mice exposed to hypoxia (Supplementary Figures E4 and E5).

Involvement of BM Cells in the Development of Hypoxia-Induced PH in n/i/eNOSs$^{-/-}$ Mice

We next examined whether BM cells were involved in the development of hypoxia-induced PH in the triply n/i/eNOSs$^{-/-}$ mice. After the normoxic exposure, there was a comparable number of circulating BM-derived VSMC progenitor cells between the WT and n/i/eNOSs$^{-/-}$ mice, as assessed by flowcytometric Sca-1^{+}/c-kit^{-}/Lin^{-} cells (29), whereas after the hypoxic exposure, there was a significant increase only in the n/i/eNOSs$^{-/-}$ mice, but not in the WT mice (Figure 4A,B). After the normoxic exposure, the serum and lung SDF-1α levels were similar between the 2 genotypes, whereas after the hypoxic exposure, both levels were significantly higher in the n/i/eNOSs$^{-/-}$ than in the WT mice (Figure 4C,D).

After the hypoxic exposure, little GFP-positive green fluorescence was seen in the lungs of WT mice transplanted with GFP-Tg-BM, whereas apparent GFP-positive green

fluorescence and GFP/α-SMA-double positive white fluorescence were detected in the lungs of n/i/eNOSs$^{-/-}$ mice transplanted with GFP-Tg-BM (Figure 4E). Quantitative analysis indicated that, after the hypoxic exposure, there were significantly more lung GFP/α-SMA-double positive cells in the n/i/eNOSs$^{-/-}$ mice, but not in the WT mice (Figure 4F).

n/i/eNOSs$^{-/-}$-BM Transplantation Exacerbates Hypoxia-Induced PH

Based on these findings, we explored the role of n/i/eNOSs in BM cells. As compared with WT mice transplanted with WT-BM, in WT mice with n/i/eNOSs$^{-/-}$-BM, the plasma NOx levels were significantly reduced by 51.6%, and the RVSP, RV/(LV+S), and medial thickness were all significantly increased (Figure 5A-D). Furthermore, as compared with n/i/eNOSs$^{-/-}$ mice transplanted with n/i/eNOSs$^{-/-}$-BM, in n/i/eNOSs$^{-/-}$ mice with WT-BM, the plasma NOx levels were significantly higher by 476.0%, and the RVSP, RV/(LV+S), and medial thickness were all significantly decreased, suggesting the involvement of n/i/eNOSs in BM cells (Figure 5A-D). As compared with the WT mice transplanted with WT-BM, in the n/i/eNOSs$^{-/-}$ mice with WT-BM, the PH parameters were significantly enhanced, and as compared with n/i/eNOSs$^{-/-}$ mice with n/i/eNOSs$^{-/-}$-BM, in the WT mice with n/i/eNOSs$^{-/-}$-BM, the PH parameters were significantly lessened, suggesting the involvement of n/i/eNOSs in non-BM cells (Figure 5A-D). n/i/eNOSs in BM and non-BM cells appeared to almost equally contribute to the development of hypoxia-induced PH. eNOS$^{-/-}$-BM or iNOS$^{-/-}$-BM transplantation did not significantly affect hypoxia-induced PH in the WT mice (Supplementary Figures 7E and 8E).

Micro CT analysis indicated that RV ejection fraction (RVEF) was significantly lower in the WT mice transplanted with n/i/eNOSs$^{-/-}$-BM as compared with those with WT-BM, without affecting LVEF or lung volume (Figure 5E,F).

Mechanisms for Exacerbation of Hypoxia-Induced PH Caused by n/i/eNOSs$^{-/-}$-BM Transplantation

We performed mRNA sequencing and analyzed 13,748 mRNAs enrolled in the reference

AJRCCM Articles in Press. Published on 26-February-2018 as 10.1164/rccm.201709-1783OC

mouse genome mm10 database. Among them, there was different expression of 2,469 mRNAs between the lungs of WT mice transplanted with WT-BM and those with n/i/eNOSs$^{-/-}$-BM after the hypoxic exposure, with statistically significant differences (P<0.05) and with more than 1.2-fold changes (n=4 each); 1,024 and 1,445 mRNAs were significantly up- and down-regulated, respectively, in the lungs of WT mice transplanted with n/i/eNOSs$^{-/-}$-BM compared with those with WT-BM.

Gene ontology analysis indicated that, in the up-regulated mRNAs, the significant biological process terms included “immune system process”, “immune response”, “innate immune response”, and “inflammation response”, suggesting the involvement of immunity and inflammation (Figure 6A and Supplementary Table E2). In the down-regulated mRNAs, the significant biological process terms included “protein folding”, “translation”, and “DNA repair”, making these results difficult to interpret (Supplementary Table E3).

Canonical pathway analysis showed that the significant terms included "nuclear factor of activated T cells signaling”, “endothelin-1 signaling”, “Wnt signaling”, “FLT3 signaling”, “Notch signaling”, “B cell receptor signaling”, “T helper cell signaling”, and “thrombin signaling” (Figure 6B). These signaling pathways are relevant to “immunity” and “inflammation”. Representative genes, including the endothelin-converting enzyme 1 and the endothelin type B receptor, are shown in Figure 6C. Mechanistic network analysis showed that the significant downstream signaling terms included “immune response of cells” and “response of antigen presenting cells”, again suggesting the involvement of “immunity” (Figure 6D).

In the lungs of WT mice transplanted with n/i/eNOSs$^{-/-}$-BM compared with those with WT-BM, 69 and 49 mRNAs categorized as “immunity” and “inflammation”, respectively, were significantly increased (Figure 7A,B). Representative genes, including complement C3, interleukin 6 receptor α, and angiotensin II type 1a receptor, are shown in Figure 7C.

We evaluated the extent of inflammation in the lung by counting the number of Mac-2-positive inflammatory cells. As compared with the WT mice transplanted with WT-BM, the number of Mac-2-positive inflammatory cells (mostly macrophages) in the lung

were significantly increased in the WT mice with n/i/eNOSs$^{-/-}$-BM and in the n/i/eNOSs$^{-/-}$ mice with WT-BM to a similar extent, and in the n/i/eNOSs$^{-/-}$ mice with n/i/eNOSs$^{-/-}$-BM to a greater extent after the hypoxic exposure (Figure 7D,E).

AJRCCM Articles in Press. Published on 26-February-2018 as 10.1164/rccm.201709-1783OC

Discussion

Inverse Association Between PASP and NOx Levels in BALF in Humans

We demonstrated in this study that higher PASP was associated with lower BALF NOx levels in patients with IPF (group 3 PH). In agreement with this evidence, it has been reported that PASP is negatively correlated with NOx levels in BALF, airway gases, and plasma of patients with idiopathic PH (group 1 PH) (32, 33). These results indicate that defective NO production is present under PH conditions. Based on this clinical outcome, we performed the basic study.

Systemic n/i/eNOSs Deficiency Promotes Development of Hypoxia-Induced PH in Mice

As compared with the WT genotype, the extents of hypoxia-induced PH were comparable in the nNOS$^{-/-}$ and iNOS$^{-/-}$ genotypes, but worsened modestly in the eNOS$^{-/-}$ genotype and markedly in the n/i/eNOSs$^{-/-}$ genotype, suggesting the protective roles of eNOS and n/i/eNOSs, but not of nNOS or iNOS, in the development of PH. eNOS in non-BM cells, but not in BM cells, seems to substantially contribute to the protective effects of n/i/eNOSs. All these abnormalities in the n/i/eNOSs$^{-/-}$ genotype were inhibited by NO supplementation with ISDN and sodium nitrate, confirming that the observed phenomena were indeed caused by defective NO production. The n/i/eNOSs$^{-/-}$ mice showed the absence of expression of all NOSs in the lung and considerably reduced the BALF NOx levels, whereas the eNOS$^{-/-}$ mice exhibited a significant and insignificant increase in expression levels of iNOS and nNOS, respectively, in the lung after the hypoxic exposure along with fairly well preserved BALF NOx levels. These results may explain in part why the n/i/eNOSs$^{-/-}$ mice developed more severe hypoxia-induced PH than the eNOS$^{-/-}$ mice. Since we did not use double NOSs$^{-/-}$ mice, the relative contribution of iNOS and nNOS to this mechanism is unknown.

Bleomycin-induced PH was also more aggravated in the n/i/eNOSs$^{-/-}$ than in the WT mice, as was the case for hypoxia-induced PH, suggesting that the n/i/eNOSs play a protective role in a broad range of PH types.

Myelocytic n/i/eNOSs Deficiency Promotes Development of Hypoxia-Induced PH in Mice

A large number of circulating BM-derived VSMC progenitor cells and enhanced plasma and lung SDF-1α levels were noted in the n/i/eNOSs$^{-/-}$ genotype exposed to hypoxia. It has been reported that BM-derived mononuclear cells differentiate into VSMC progenitor cells and contribute to vascular lesion formation (34, 35), and that the CXC chemokine SDF-1α is a pivotal chemotactic factor of the BM-derived VSMC progenitor cells (36). It is therefore likely that SDF-1α-induced recruitment of circulating BM-derived VSMC progenitor cells was involved in the pulmonary vascular remodeling observed in the n/i/eNOSs$^{-/-}$ genotype exposed to hypoxia. We obtained further direct evidence of GFP/α-SMA-double positive white fluorescence in the thickened media of the small pulmonary arteries in the n/i/eNOSs$^{-/-}$ mice transplanted with GFP-Tg-BM after the hypoxic exposure. It is thus evident that BM cells were involved in the development of hypoxia-induced PH in the n/i/eNOSs$^{-/-}$ genotype.

On the basis of these results, we explored the role of n/i/eNOSs in BM cells in the development of PH. There were lower levels of plasma NOx in the WT genotype transplanted with n/i/eNOSs$^{-/-}$-BM as compared with those with WT-BM. Surprisingly, approximately 50% of systemic NO production appears to be derived from BM cells. n/i/eNOSs$^{-/-}$-BM transplantation deteriorated the hypoxia-induced PH in the WT genotype, and WT-BM transplantation ameliorated the hypoxia-induced PH in the n/i/eNOSs$^{-/-}$-genotype. This is the first experimental demonstration showing that myelocytic n/i/eNOSs exert inhibitory effects against the development of PH. The n/i/eNOSs$^{-/-}$-BM transplantation reduced RVEF but did not affect LVEF in the WT genotype. It is thus possible that the observed alterations were not due to left heart failure (group 2 PH).

Immune and Inflammatory Mechanisms Mediate the Promotion of Hypoxia-Induced PH Caused by Myelocytic n/i/eNOSs Deficiency

We performed mRNA sequencing using a next-generation sequencer in order to examine the mechanisms involved in the deterioration of hypoxia-induced PH caused by myelocytic n/i/eNOSs deficiency. Intriguingly, even though the lung tissues were derived from the

AJRCCM Articles in Press. Published on 26-February-2018 as 10.1164/rccm.201709-1783OC

same WT mice, n/i/eNOSs$^{-/-}$-BM transplantation significantly changed very many genes of the 3,251 mRNAs as compared with WT-BM transplantation. These results further support the important role of myelocytic n/i/eNOSs in the development of PH. The software analyses concordantly indicated that the n/i/eNOSs$^{-/-}$-BM transplantation increased the expression of genes related to "immunity" and "inflammation". Consistent with these results, as compared with WT mice transplanted with WT-BM, the number of inflammatory cells was increased in the WT mice with n/i/eNOSs$^{-/-}$-BM and in the n/i/eNOSs$^{-/-}$ mice with WT-BM to a similar extent, and in the n/i/eNOSs$^{-/-}$ mice with n/i/eNOSs$^{-/-}$-BM to a greater extent, suggesting the involvement of inflammation in the exacerbation of hypoxia-induced PH caused by n/i/eNOSs deficiency in BM and non-BM cells.

Conclusions

We were able to demonstrate that higher PASP was associated with lower BALF NOx levels in patients with IPF, and that the presence or absence of n/i/eNOSs in BM cells modulated the severity of hypoxia-induced PH in mice via the immune and inflammatory pathways, indicating a novel protective role of n/i/eNOSs, specifically in BM cells, in the pathogenesis of PH. Our findings should contribute to a better understanding of the cellular and molecular basis of this fatal pulmo-vascular disorder.

References

1. Strange G, Playford D, Stewart S, Deague JA, Nelson H, Kent A, Gabbay E. Pulmonary hypertension: prevalence and mortality in the Armadale echocardiography cohort. *Heart* 2012; 98: 1805-1811.
2. Hurdman J, Condliffe R, Elliot CA, Davies C, Hill C, Wild JM, Capener D, Sephton P, Hamilton N, Armstrong IJ, Billings C, Lawrie A, Sabroe I, Akil M, O'Toole L, Kiely DG. ASPIRE registry: assessing the Spectrum of Pulmonary hypertension Identified at a REferral centre. *Eur Respir J* 2012; 39: 945-955.
3. National Cancer Institute: Surveilllance, epidemiology, and end results (SEER) program website, cancer statistics review. date last updated: September 12, 2016.
4. Chin K, Channick RN. Pulmonary Hypertension. In: Broaddus VC, Mason RJ, Ernst JD, King JTE, Lazarus SC, Murray JF, Nadel JA, Slutsky AS, editors. Murray & Nadel's Textbook of Respiratory Medicine, Sixth Edition ed. Philadelphia: Elsevier; 2015. p. 1031-1049.
5. Brindicci C, Kharitonov SA, Ito M, Elliott MW, Hogg JC, Barnes PJ, Ito K. Nitric oxide synthase isoenzyme expression and activity in peripheral lung tissue of patients with chronic obstructive pulmonary disease. *Am J Respir Crit Care Med* 2010; 181: 21-30.
6. Tsutsui M, Shimokawa H, Otsuji Y, Yanagihara N. Pathophysiological relevance of NO signaling in the cardiovascular system: novel insight from mice lacking all NO synthases. *Pharmacol Ther* 2010; 128: 499-508.
7. Tsutsui M, Tanimoto A, Tamura M, Mukae H, Yanagihara N, Shimokawa H, Otsuji Y. Significance of nitric oxide synthases: Lessons from triple nitric oxide synthases null mice. *J Pharmacol Sci* 2015; 127: 42-52.
8. Buchwalow IB, Podzuweit T, Bocker W, Samoilova VE, Thomas S, Wellner M, Baba HA, Robenek H, Schnekenburger J, Lerch MM. Vascular smooth muscle and nitric oxide synthase. *FASEB J* 2002; 16: 500-508.
9. Kobzik L, Bredt DS, Lowenstein CJ, Drazen J, Gaston B, Sugarbaker D, Stamler JS.

AJRCCM Articles in Press. Published on 26-February-2018 as 10.1164/rccm.201709-1783OC

Nitric oxide synthase in human and rat lung: immunocytochemical and histochemical localization. *Am J Respir Cell Mol Biol* 1993; 9: 371-377.

10. Seimetz M, Parajuli N, Pichl A, Veit F, Kwapiszewska G, Weisel FC, Milger K, Egemnazarov B, Turowska A, Fuchs B, Nikam S, Roth M, Sydykov A, Medebach T, Klepetko W, Jaksch P, Dumitrascu R, Garn H, Voswinckel R, Kostin S, Seeger W, Schermuly RT, Grimminger F, Ghofrani HA, Weissmann N. Inducible NOS inhibition reverses tobacco-smoke-induced emphysema and pulmonary hypertension in mice. *Cell* 2011; 147: 293-305.
11. Hampl V, Bibova J, Banasova A, Uhlik J, Mikova D, Hnilickova O, Lachmanova V, Herget J. Pulmonary vascular iNOS induction participates in the onset of chronic hypoxic pulmonary hypertension. *Am J Physiol Lung Cell Mol Physiol* 2006; 290: L11-20.
12. Fagan KA, Tyler RC, Sato K, Fouty BW, Morris KG, Jr., Huang PL, McMurtry IF, Rodman DM. Relative contributions of endothelial, inducible, and neuronal NOS to tone in the murine pulmonary circulation. *Am J Physiol* 1999; 277: L472-478.
13. Ozaki M, Kawashima S, Yamashita T, Ohashi Y, Rikitake Y, Inoue N, Hirata KI, Hayashi Y, Itoh H, Yokoyama M. Reduced hypoxic pulmonary vascular remodeling by nitric oxide from the endothelium. *Hypertension* 2001; 37: 322-327.
14. Steudel W, Scherrer-Crosbie M, Bloch KD, Weimann J, Huang PL, Jones RC, Picard MH, Zapol WM. Sustained pulmonary hypertension and right ventricular hypertrophy after chronic hypoxia in mice with congenital deficiency of nitric oxide synthase 3. *J Clin Invest* 1998; 101: 2468-2477.
15. Quinlan TR, Li D, Laubach VE, Shesely EG, Zhou N, Johns RA. eNOS-deficient mice show reduced pulmonary vascular proliferation and remodeling to chronic hypoxia. *Am J Physiol Lung Cell Mol Physiol* 2000; 279: L641-650.
16. Hampl V, Herget J. Role of nitric oxide in the pathogenesis of chronic pulmonary hypertension. *Physiol Rev* 2000; 80: 1337-1372.
17. Morishita T, Tsutsui M, Shimokawa H, Sabanai K, Tasaki H, Suda O, Nakata S, Tanimoto A, Wang KY, Ueta Y, Sasaguri Y, Nakashima Y, Yanagihara N. Nephrogenic

diabetes insipidus in mice lacking all nitric oxide synthase isoforms. *Proc Natl Acad Sci U S A* 2005; 102: 10616-10621.

18. Farha S, Asosingh K, Xu W, Sharp J, George D, Comhair S, Park M, Tang WH, Loyd JE, Theil K, Tubbs R, Hsi E, Lichtin A, Erzurum SC. Hypoxia-inducible factors in human pulmonary arterial hypertension: a link to the intrinsic myeloid abnormalities. *Blood* 2011; 117: 3485-3493.
19. Adir Y, Elia D, Harari S. Pulmonary hypertension in patients with chronic myeloproliferative disorders. *Eur Respir Rev* 2015; 24: 400-410.
20. Yan L, Chen X, Talati M, Nunley BW, Gladson S, Blackwell T, Cogan J, Austin E, Wheeler F, Loyd J, West J, Hamid R. Bone Marrow-derived Cells Contribute to the Pathogenesis of Pulmonary Arterial Hypertension. *Am J Respir Crit Care Med* 2016; 193: 898-909.
21. Tsutsui M, Ogoshi T, Kido T, Yamada S, Wang K, Toyohira Y, Shimokawa H, Yanagihara N, Yatera K, Mukae H. Protective role of myelocytic nitric oxide synthases in hypoxic pulmonary hypertension in mice. *Circulation* 2017; 136: A17700.
22. Brittain EL, Duncan MS, Chang J, Patterson OV, DuVall SL, Brandt CA, So-Armah KA, Goetz M, Akgun K, Crothers K, Zola C, Kim J, Gibert C, Pisani M, Morris A, Hsue P, Tindle HA, Justice A, Freiberg M. Increased Echocardiographic Pulmonary Pressure in HIV-infected and Uninfected Individuals in the Veterans Aging Cohort Study. *Am J Respir Crit Care Med* 2017.
23. Kircher BJ, Himelman RB, Schiller NB. Noninvasive estimation of right atrial pressure from the inspiratory collapse of the inferior vena cava. *Am J Cardiol* 1990; 66: 493-496.
24. Sakamoto N, Mukae H, Fujii T, Kakugawa T, Kaida H, Kadota J, Kohno S. Soluble form of Fas and Fas ligand in serum and bronchoalveolar lavage fluid of individuals infected with human T-lymphotropic virus type 1. *Respir Med* 2004; 98: 213-219.
25. Kina-Tanada M, Sakanashi M, Tanimoto A, Kaname T, Matsuzaki T, Noguchi K, Uchida T, Nakasone J, Kozuka C, Ishida M, Kubota H, Taira Y, Totsuka Y, Kina SI,

AJRCCM Articles in Press. Published on 26-February-2018 as 10.1164/rccm.201709-1783OC

Sunakawa H, Omura J, Satoh K, Shimokawa H, Yanagihara N, Maeda S, Ohya Y, Matsushita M, Masuzaki H, Arasaki A, Tsutsui M. Long-term dietary nitrite and nitrate deficiency causes the metabolic syndrome, endothelial dysfunction and cardiovascular death in mice. *Diabetologia* 2017; 60: 1138-1151.

26. Morisada N, Nomura M, Nishii H, Furuno Y, Sakanashi M, Sabanai K, Toyohira Y, Ueno S, Watanabe S, Tamura M, Matsumoto T, Tanimoto A, Sasaguri Y, Shimokawa H, Kusuhara K, Yanagihara N, Shirahata A, Tsutsui M. Complete disruption of all nitric oxide synthase genes causes markedly accelerated renal lesion formation following unilateral ureteral obstruction in mice in vivo. *J Pharmacol Sci* 2010; 114: 379-389.

27. Furuno Y, Morishita T, Toyohira Y, Yamada S, Ueno S, Morisada N, Sugita K, Noguchi K, Sakanashi M, Miyata H, Tanimoto A, Sasaguri Y, Shimokawa H, Otsuji Y, Yanagihara N, Tamura M, Tsutsui M. Crucial vasculoprotective role of the whole nitric oxide synthase system in vascular lesion formation in mice: Involvement of bone marrow-derived cells. *Nitric Oxide* 2011; 25: 350-359.

28. Noguchi S, Yatera K, Wang KY, Oda K, Akata K, Yamasaki K, Kawanami T, Ishimoto H, Toyohira Y, Shimokawa H, Yanagihara N, Tsutsui M, Mukae H. Nitric oxide exerts protective effects against bleomycin-induced pulmonary fibrosis in mice. *Respir Res* 2014; 15: 92.

29. Uchida T, Furuno Y, Tanimoto A, Toyohira Y, Arakaki K, Kina-Tanada M, Kubota H, Sakanashi M, Matsuzaki T, Noguchi K, Nakasone J, Igarashi T, Ueno S, Matsushita M, Ishiuchi S, Masuzaki H, Ohya Y, Yanagihara N, Shimokawa H, Otsuji Y, Tamura M, Tsutsui M. Development of an experimentally useful model of acute myocardial infarction: 2/3 nephrectomized triple nitric oxide synthases-deficient mouse. *J Mol Cell Cardiol* 2014; 77: 29-41.

30. Sasaguri Y, Wang KY, Tanimoto A, Tsutsui M, Ueno H, Murata Y, Kohno Y, Yamada S, Ohtsu H. Role of histamine produced by bone marrow-derived vascular cells in pathogenesis of atherosclerosis. *Circ Res* 2005; 96: 974-981.

31. Xu W, Kaneko FT, Zheng S, Comhair SA, Janocha AJ, Goggans T, Thunnissen FB,

Farver C, Hazen SL, Jennings C, Dweik RA, Arroliga AC, Erzurum SC. Increased arginase II and decreased NO synthesis in endothelial cells of patients with pulmonary arterial hypertension. *FASEB J* 2004; 18: 1746-1748.

32. Kaneko FT, Arroliga AC, Dweik RA, Comhair SA, Laskowski D, Oppedisano R, Thomassen MJ, Erzurum SC. Biochemical reaction products of nitric oxide as quantitative markers of primary pulmonary hypertension. *Am J Respir Crit Care Med* 1998; 158: 917-923.

33. Zhang R, Wang XJ, Zhang HD, Sun XQ, Zhao QH, Wang L, He J, Jiang X, Liu JM, Jing ZC. Profiling nitric oxide metabolites in patients with idiopathic pulmonary arterial hypertension. *Eur Respir J* 2016; 48: 1386-1395.

34. Sata M, Saiura A, Kunisato A, Tojo A, Okada S, Tokuhisa T, Hirai H, Makuuchi M, Hirata Y, Nagai R. Hematopoietic stem cells differentiate into vascular cells that participate in the pathogenesis of atherosclerosis. *Nat Med* 2002; 8: 403-409.

35. Shimizu K, Sugiyama S, Aikawa M, Fukumoto Y, Rabkin E, Libby P, Mitchell RN. Host bone-marrow cells are a source of donor intimal smooth- muscle-like cells in murine aortic transplant arteriopathy. *Nat Med* 2001; 7: 738-741.

36. Ceradini DJ, Kulkarni AR, Callaghan MJ, Tepper OM, Bastidas N, Kleinman ME, Capla JM, Galiano RD, Levine JP, Gurtner GC. Progenitor cell trafficking is regulated by hypoxic gradients through HIF-1 induction of SDF-1. *Nat Med* 2004; 10: 858-864.

AJRCCM Articles in Press. Published on 26-February-2018 as 10.1164/rccm.201709-1783OC

Figure Legends

Figure 1

An inverse correlation between pulmonary artery systolic pressure and NOx (nitrite plus nitrate), nitrate, or nitrite levels in BALF in patients with idiopathic pulmonary fibrosis. Pulmonary artery systolic pressure estimated by Doppler echocardiography was significantly and negatively correlated with NOx and nitrate concentrations in BALF in patients with idiopathic pulmonary fibrosis.

Figure 2

NOx levels in plasma and BALF and NO synthase (NOS) expression levels in the lung in wild-type (WT), single NOS$^{-/-}$, and triple n/i/eNOSs$^{-/-}$ mice exposed to normoxia or hypoxia. (**A, B**) NOx levels in the plasma (n=7-10) and BALF (n=4-7) after the normoxic and hypoxic exposure. **P*<0.05 vs. WT mice. †*P*<0.05 vs. normoxia. (**C-F**) NOS isoform expression levels in the lung after the normoxic and hypoxic exposure (n=4-5). **P*<0.05 vs. WT mice after the hypoxic exposure. †*P*<0.05 vs. normoxia.

Figure 3

Survival rate, right ventricular systolic pressure (RVSP), right ventricular hypertrophy, and pulmonary vascular remodeling in WT, single NOS$^{-/-}$, and triple n/i/eNOSs$^{-/-}$ mice exposed to normoxia or hypoxia. (**A**) Survival rate after the hypoxic exposure (n=14-34). **P*<0.05 vs. WT; †*P*<0.05 vs. eNOS$^{-/-}$. (**B**) Representative tracing of RVSP (scale bar=0.1 sec). (**C**) RVSP after the normoxic and hypoxic exposure. (**D**) Hematoxylin and eosin (H&E) staining of heart cross-sections. Scale bar=1mm. (**E**) Weight ratio of the right ventricle to the left ventricle plus the interventricular septum (RV/[LV+S]) after the normoxic and hypoxic exposure. **P*<0.05 vs. normoxia; †*P*<0.05 vs. WT; ‡ vs. eNOS$^{-/-}$. (**F**) H&E, elastic van Gieson (EVG), and α-smooth muscle actin (α-SMA) staining of small pulmonary arteries. Scale bar=50 μm. (**G**) Medial thickness of small pulmonary arteries (50-150 μm in diameter) (n=5-10). **P*<0.05 vs. normoxia; †*P*<0.05 vs. WT; ‡ vs. eNOS$^{-/-}$.

Figure 4

Involvement of bone marrow (BM) cells and stromal cell-derived factor (SDF)-1α in hypoxia-induced PH in n/i/eNOSs$^{-/-}$ mice. (**A**, **B**) Circulating stem cell antigen-1^{+} (Sca-1^{+})/c-kit^{-}/lineage (Lin)$^{-}$ cells (interpreted as BM-derived vascular smooth muscle cell [VSMC] progenitor cells) assessed by flowcytometry (n=5). **P*<0.05 vs. normoxia. (**C**, **D**) Serum and lung SDF-1α levels (n=5). **P*<0.05 vs. normoxia; †*P*<0.05 vs. WT mice. (**E**) Immunofluorescent staining in the lung of WT and n/i/eNOSs$^{-/-}$ mice transplanted with BM cells isolated from green fluorescent protein-transgenic (GFP-Tg) mice after the hypoxic exposure. Apparent GFP-positive green fluorescence and GFP/SMA-double positive white fluorescence were observed (n=5). DAPI, 4',6-diamidino-2-phenylindole (nuclear staining). Bars = 50 μm. (**F**) The number of GFP/α-SMA-double positive cells (% in total α-SMA-positive cells). **P*<0.05 vs. normoxia.

Figure 5

Plasma NOx levels, hypoxia-induced PH, and cardiac function in WT and n/i/eNOSs$^{-/-}$ mice transplanted with either WT or n/i/eNOSs$^{-/-}$ BM cells. (**A-D**) Plasma NOx levels after the hypoxic exposure and hypoxia-induced PH (n=5-6). **P*<0.05 vs. WT mice transplanted with WT-BM; †*P*<0.05 vs. n/i/eNOSs$^{-/-}$ mice transplanted with n/i/eNOSs$^{-/-}$-BM. (**E**) Micro computed tomography (CT) images. (**F**) Left ventricular ejection fraction (LVEF), right ventricular ejection fraction (RVEF), and lung volume after the hypoxic exposure (n=4). **P*<0.05.

Figure 6

Systemic pathway analysis of differentially expressed genes between the lungs of WT mice transplanted with WT-BM and those with n/i/eNOSs$^{-/-}$-BM. mRNA sequencing was performed with a next-generation sequencer, and 3,251 mRNAs were differentially expressed between the lungs of WT mice transplanted with WT-BM and those with n/i/eNOSs$^{-/-}$-BM after the hypoxic exposure with statistically significant differences (*P*<0.05)

AJRCCM Articles in Press. Published on 26-February-2018 as 10.1164/rccm.201709-1783OC

and with more than 1.2-fold changes (n=4 each); 1,024 and 1,445 mRNAs were significantly up- and down-regulated, respectively, in the lungs of WT mice transplanted with n/i/eNOSs$^{-/-}$-BM. (**A**) Significant biological process terms detected by gene ontology (GO) analysis of the software of database for annotation, visualization, and integrated discovery (DAVID). (**B**) Significant terms detected by the software of ingenuity pathways analysis (IPA). Bars indicate -log(*P*-value), and orange and blue bars stand for up- and down-regulated pathways, respectively. The line represents the ratio of the number of significantly expressed mRNAs to the number of genes listed in each pathway. The DAVID and IPA softwares concordantly indicated that the n/i/eNOSs$^{-/-}$-BM transplantation increased genes related to "immunity" and "inflammation". (**C**) Representative genes in significant terms detected by the Canonical analysis of IPA software. ECE, endothelin converting enzyme 1; ET-B, endothelin receptor type B; CD28, CD28 antigen; STAT, signal transducer and activator of transcription; BCL, B cell leukemia/lymphoma; MAPK, mitogen-activated protein kinase; MEF, myocyte enhancer factor; PLC, phospholipase C; WNT, wingless-type MMTV integration site family member; ARHGEF, Rho guanine nucleotide exchange factor (GEF); FGF-R, fibroblast growth factor receptor; FLT3L, FMS-like tyrosine kinase 3 ligand; PDPK, 3-phosphoinositide dependent protein kinase. **P*<0.05. FPKM=fragments per kilobase of exon per million mapped fragments. (**D**) Significant terms detected by downstream effect analysis.

Figure 7

Differentially expressed immunity- and inflammation-related genes and inflammatory cell infiltration between the lungs of WT mice transplanted with WT-BM and those with n/i/eNOSs$^{-/-}$-BM. (**A, B**) Heat maps of differentially expressed mRNAs categorized as immunity and inflammation in the Subio platform. (**C**) Representative genes in the differentially expressed mRNAs. C, complement component; AT_{1a}-R, angiotensin II type 1a receptor; IL6-Rα, interleukin 6 receptor alpha; MMP, matrix metalloproteinase; CCL, chemokine (C-C motif) ligand; CXCR, chemokine (C-X-C motif) receptor; ECM, extracellular matrix protein; TLR, toll-like receptor; NLRP3, NLR family, pyrin domain

containing 3. *P<0.05. (**D**) Representative Mac-2 immunostaining in the lung after the hypoxic exposure. Arrows indicate Mac-2-positive cells. Scale bar=50 μm. (**E**) The number of Mac-2-positive inflammatory cells in the lung after the hypoxic exposure (n=4). *P<0.05 vs. WT mice transplanted with WT-BM; †P<0.05 vs. n/i/eNOSs$^{-/-}$ mice with n/i/eNOSs$^{-/-}$-BM.

AJRCCM Articles in Press. Published on 26-February-2018 as 10.1164/rccm.201709-1783OC

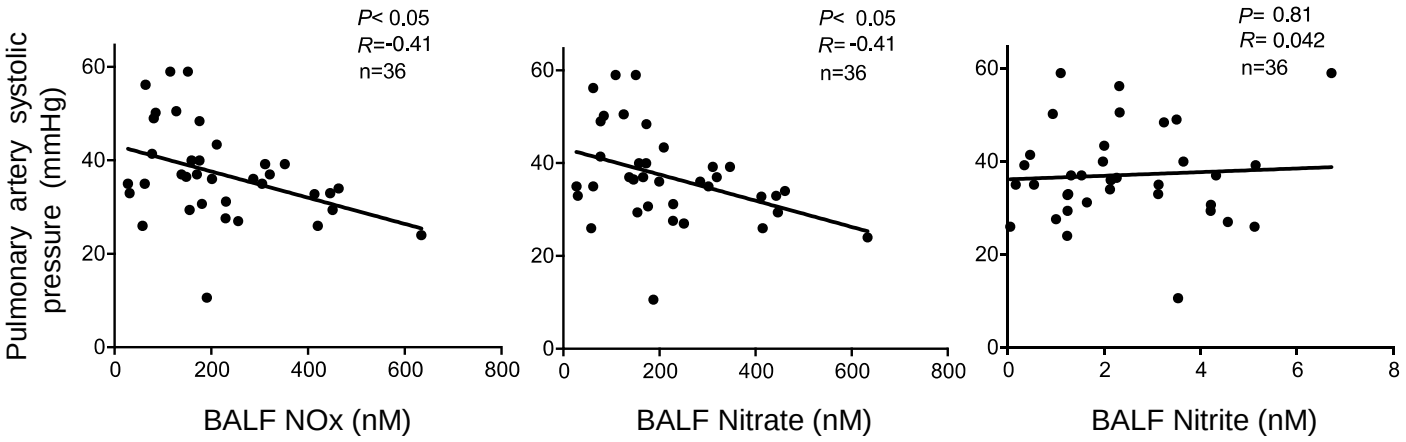

Figure 1

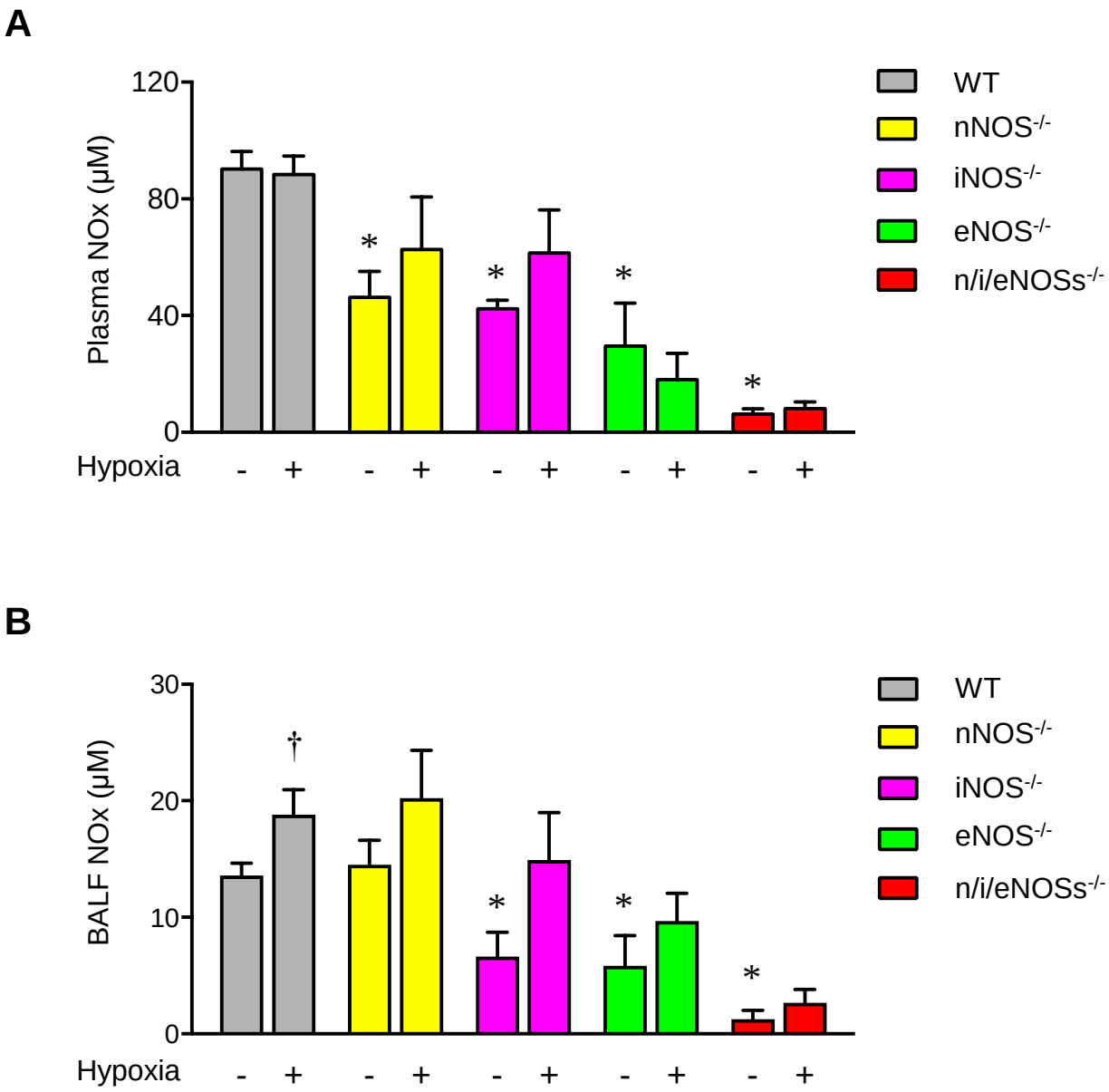

Figure 2 A,B

AJRCCM Articles in Press. Published on 26-February-2018 as 10.1164/rccm.201709-1783OC

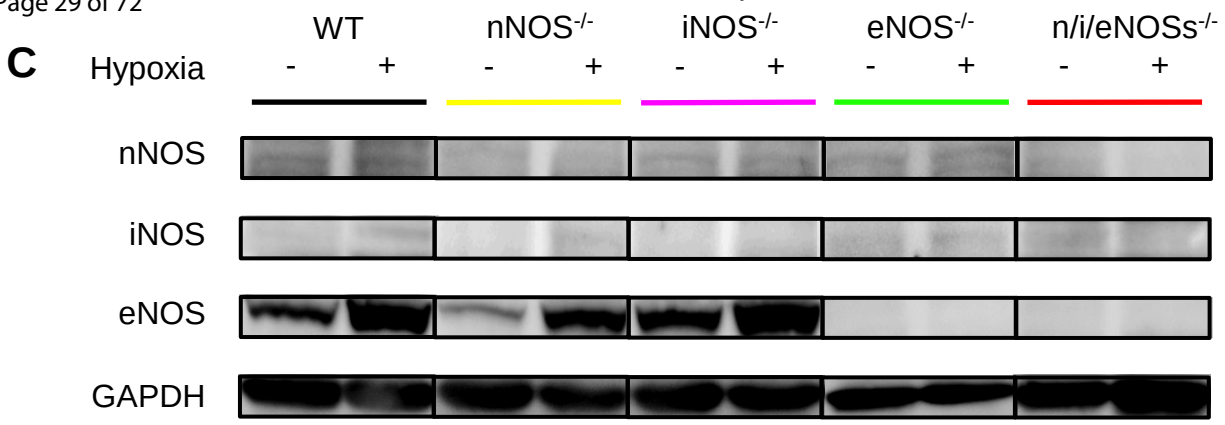

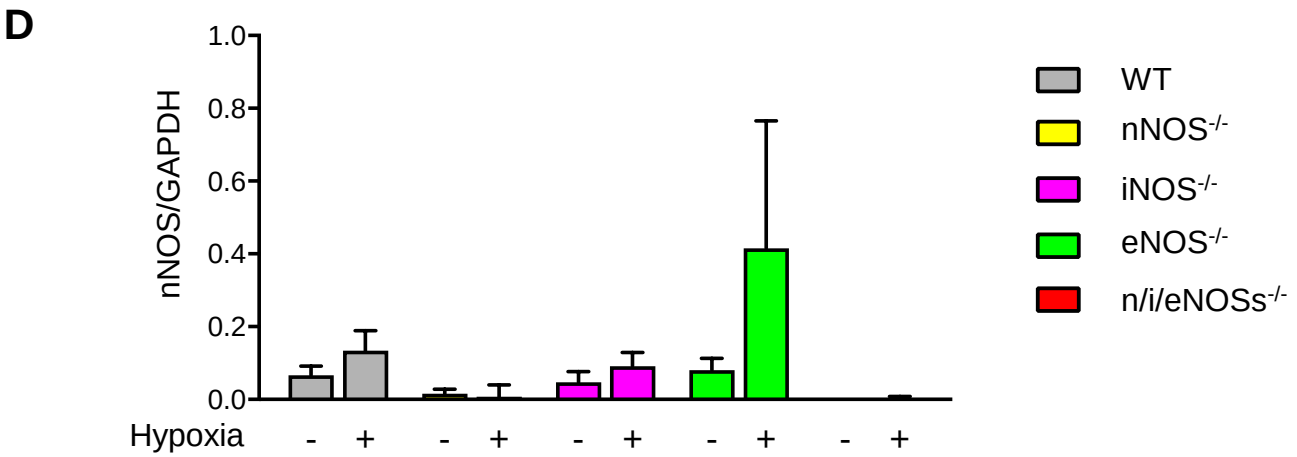

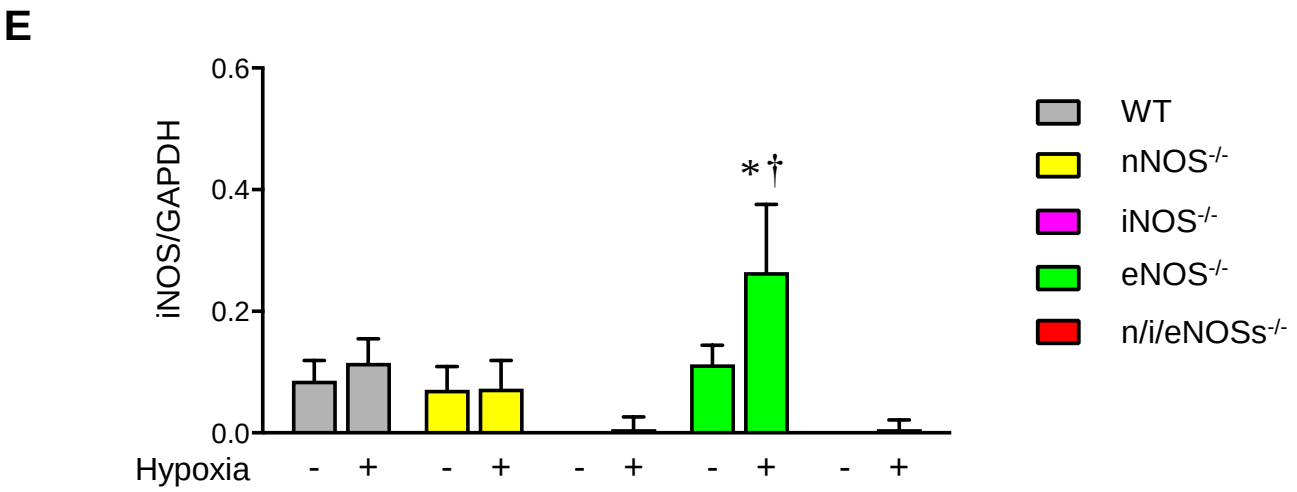

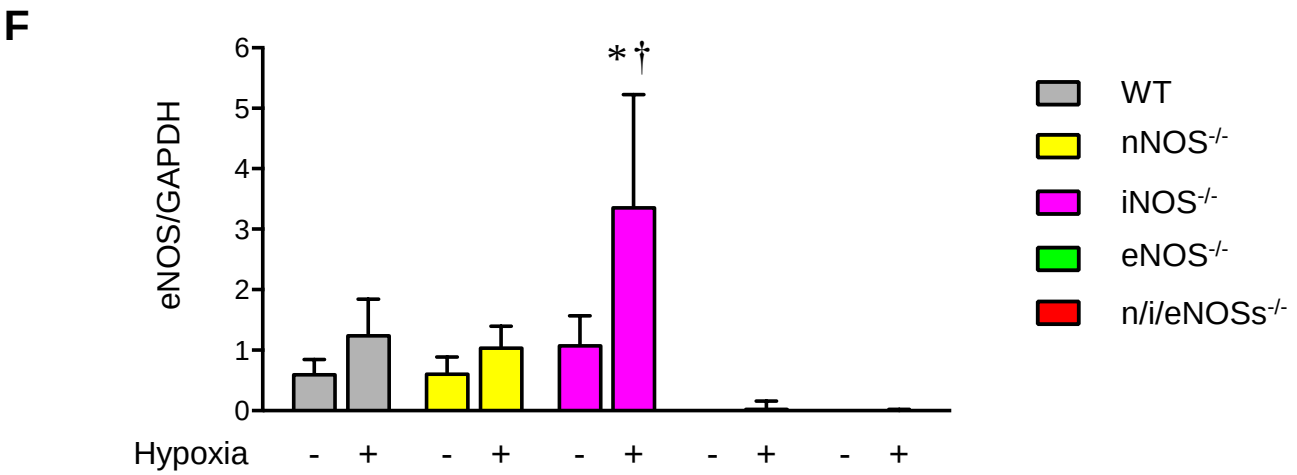

Figure 2 C-F

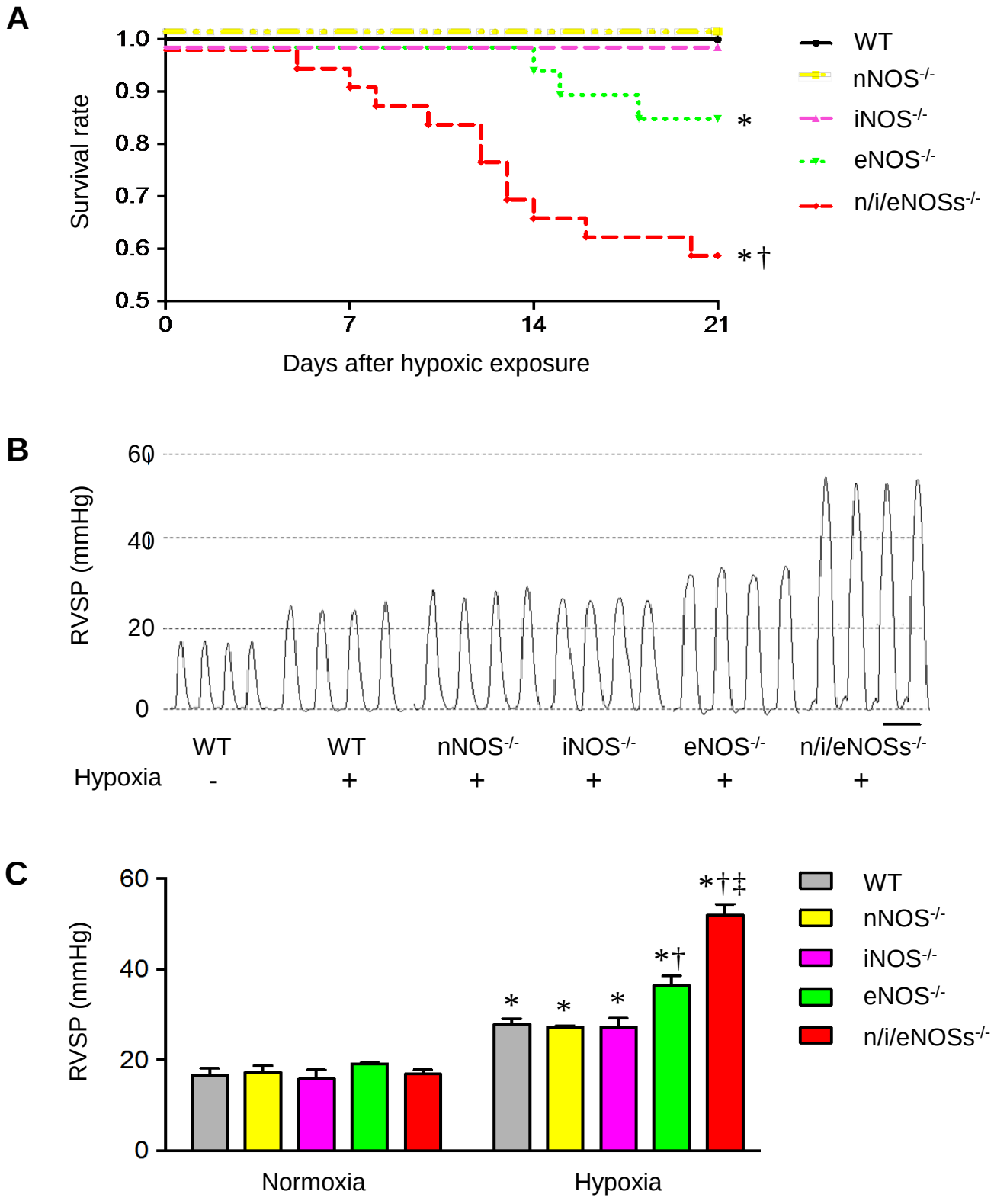

Figure 3 A-C

AJRCCM Articles in Press. Published on 26-February-2018 as 10.1164/rccm.201709-1783OC

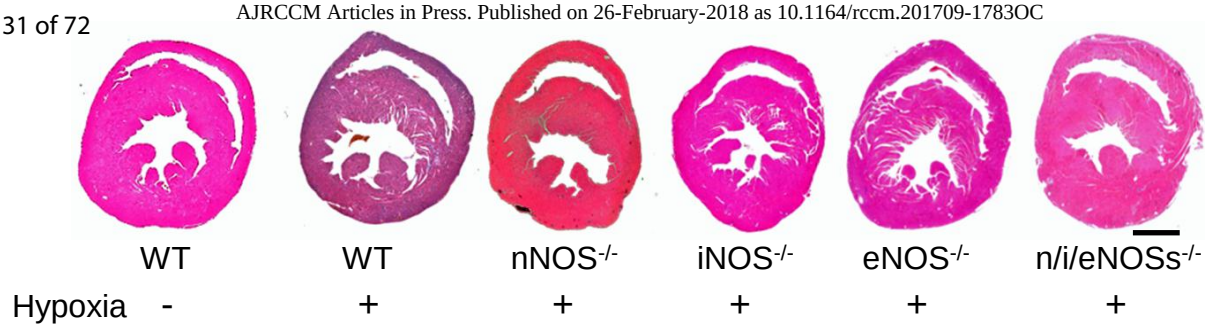

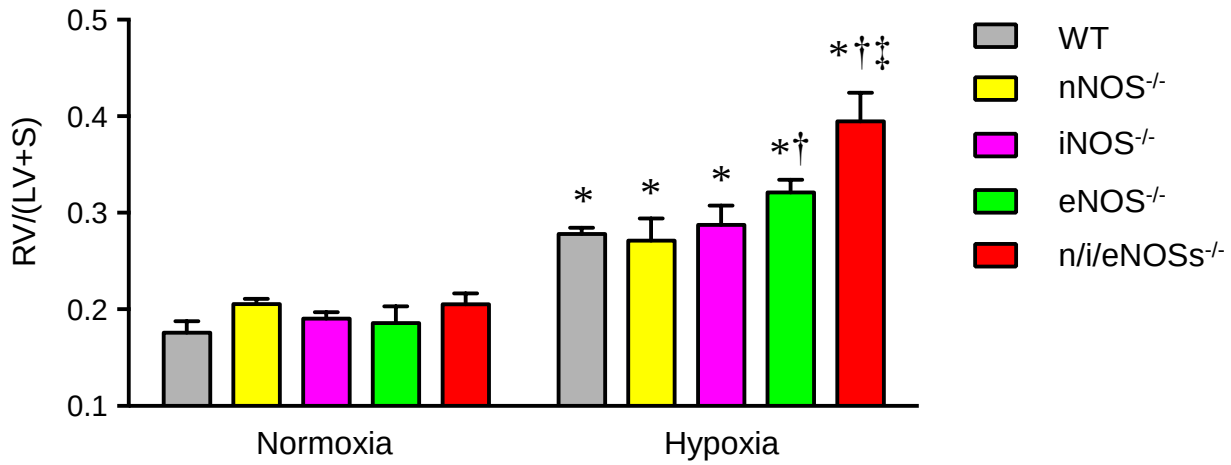

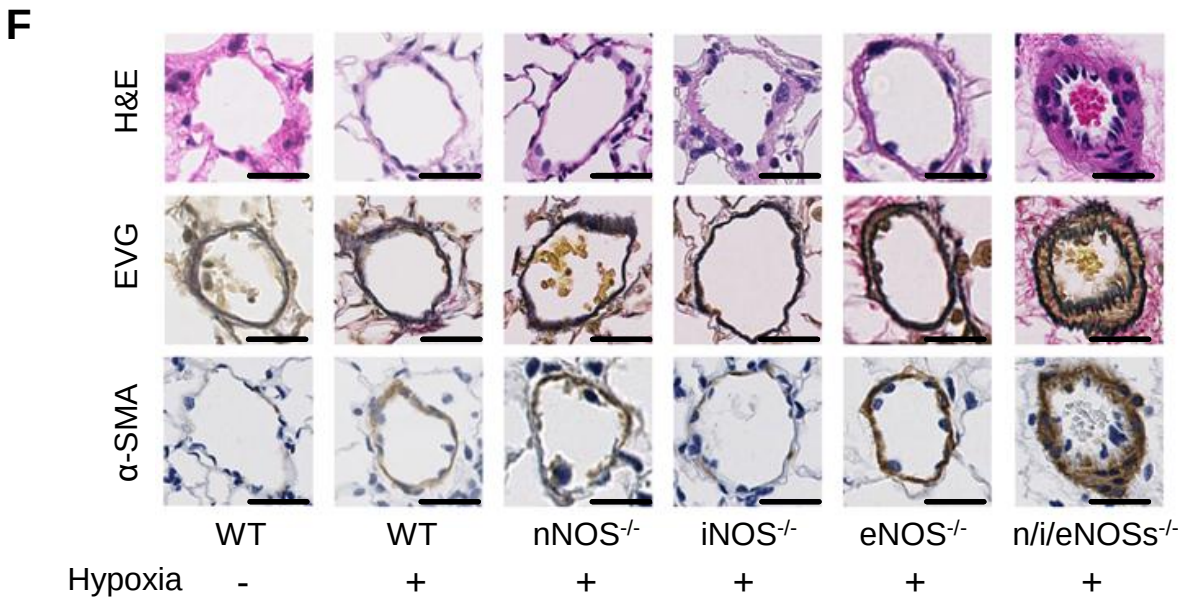

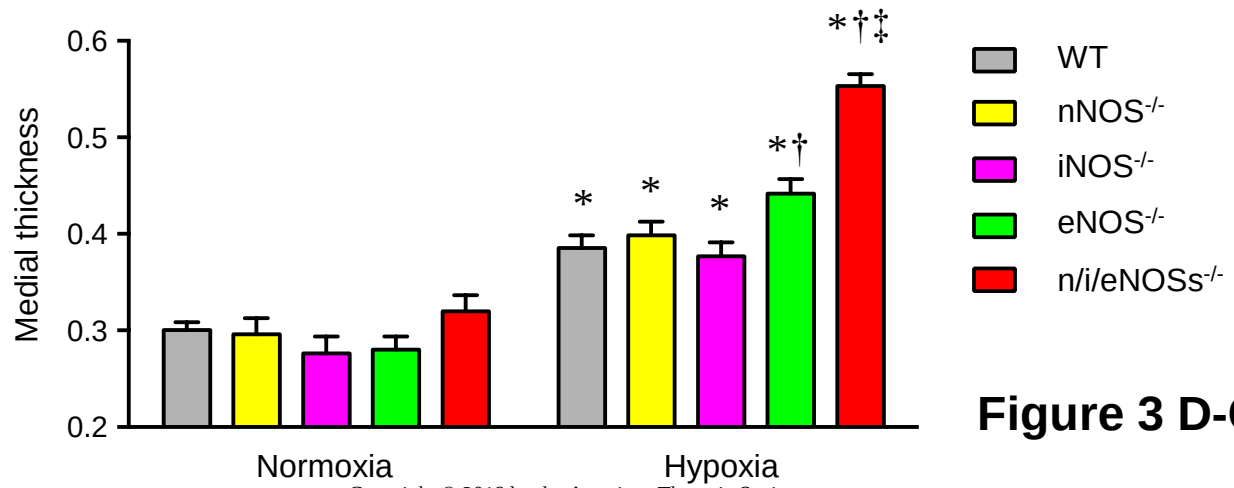

Figure 3 D-G

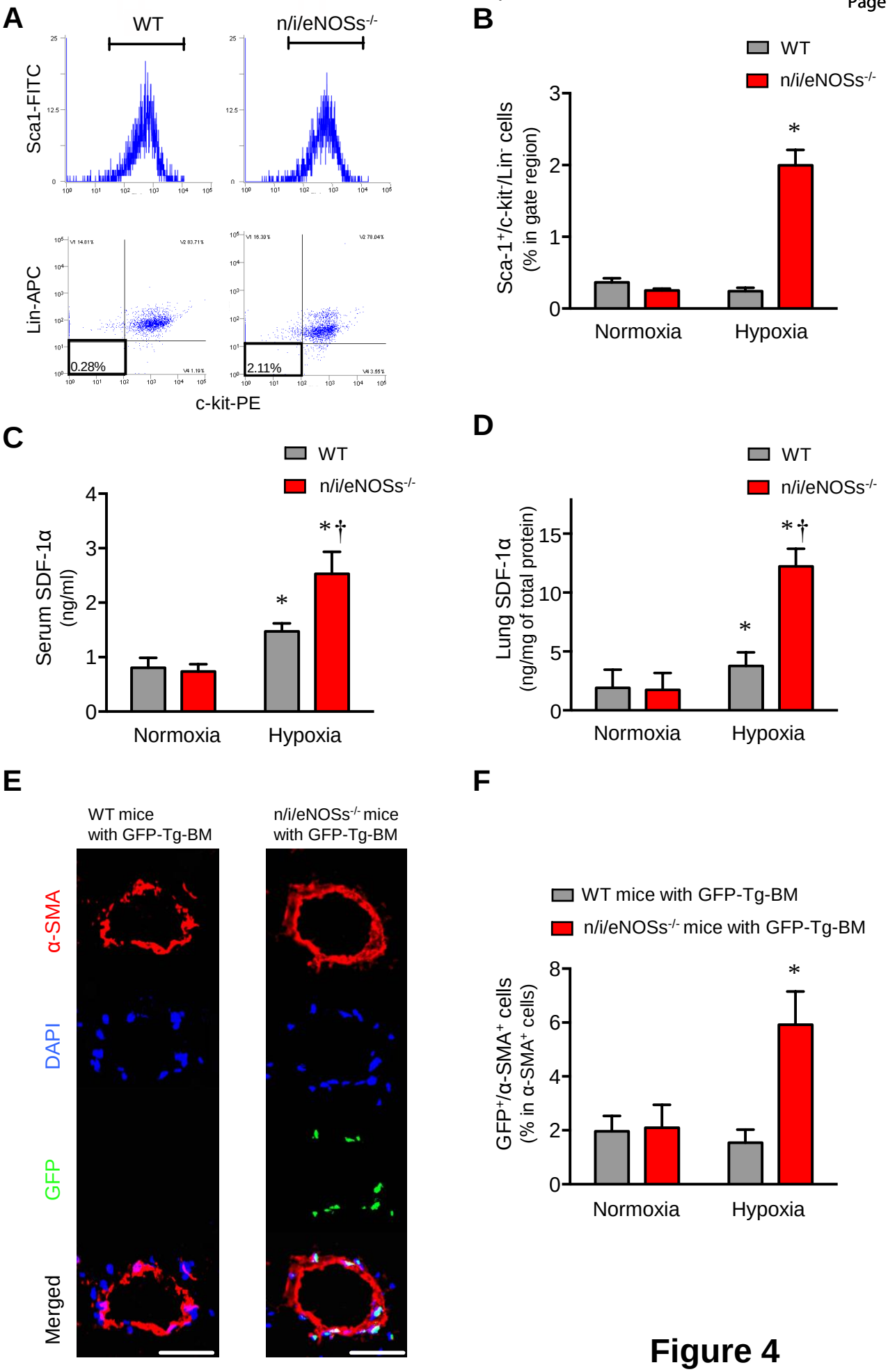

Figure 4

AJRCCM Articles in Press. Published on 26-February-2018 as 10.1164/rccm.201709-1783OC

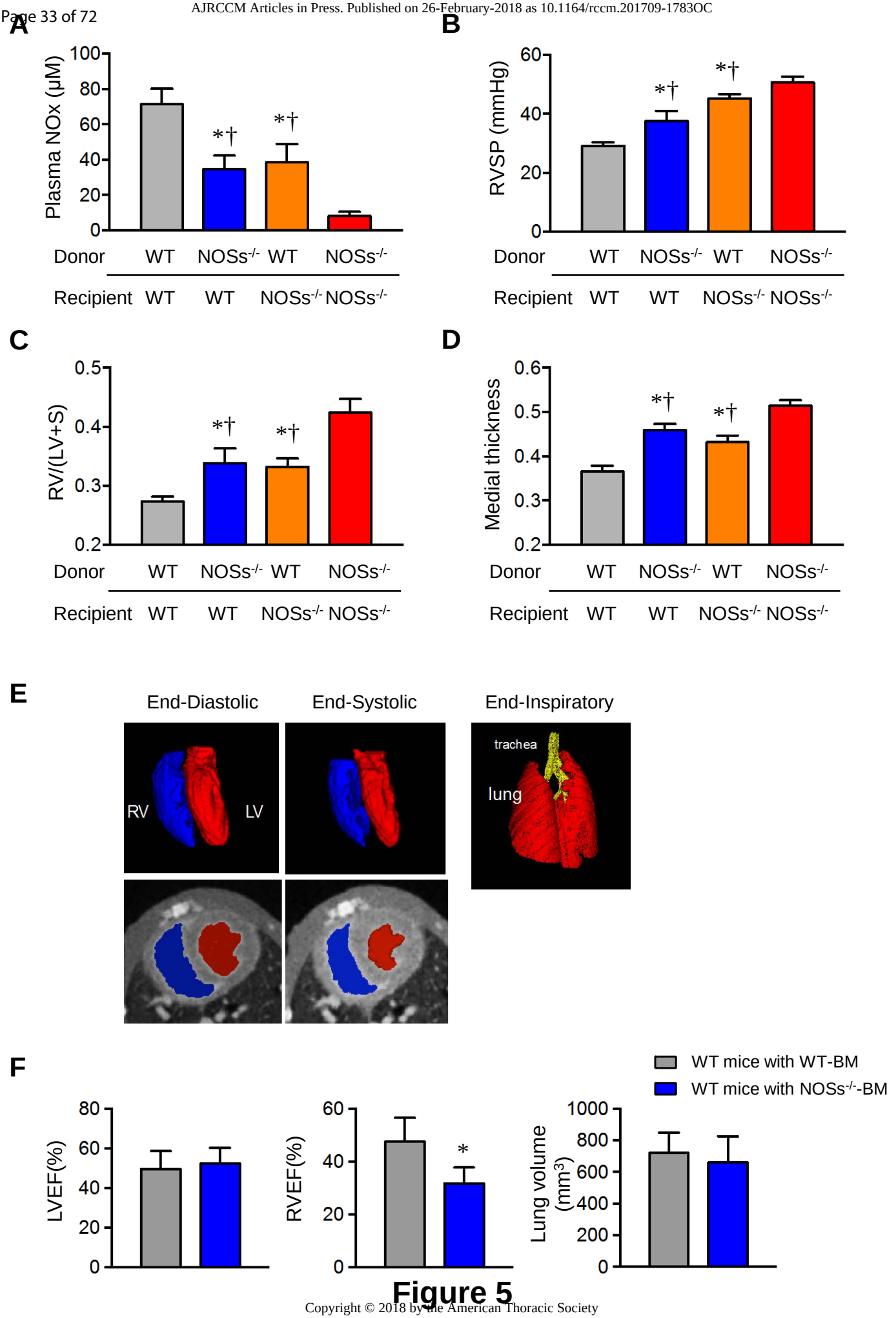

Figure 5

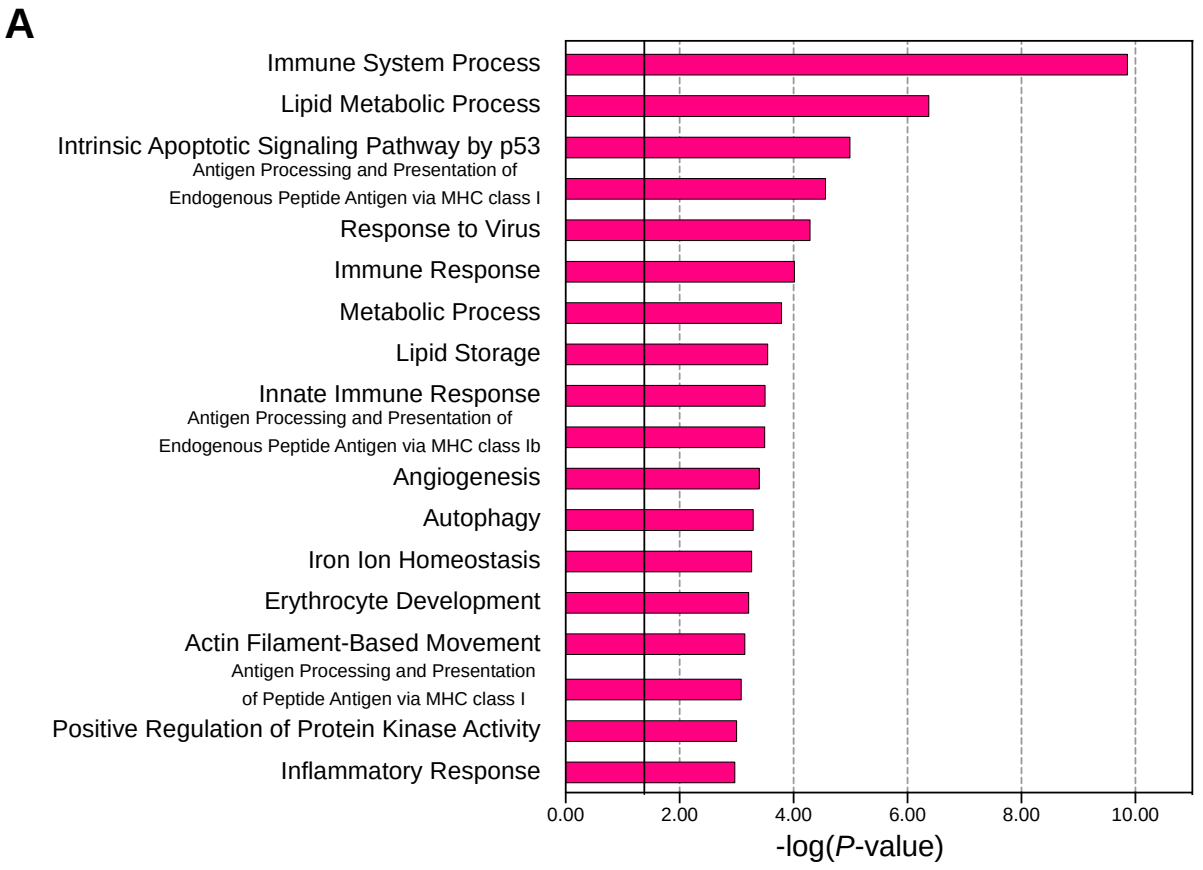

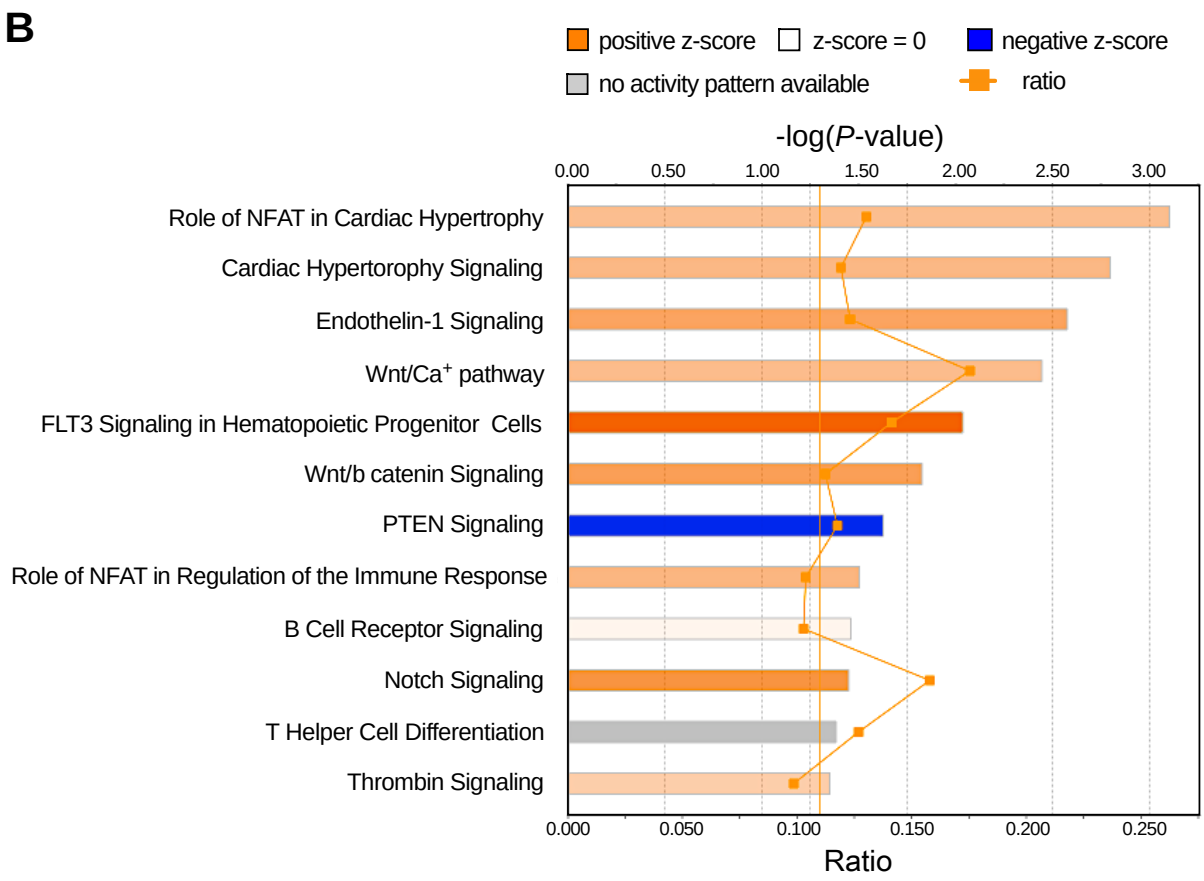

Figure 6 A,B

AJRCCM Articles in Press. Published on 26-February-2018 as 10.1164/rccm.201709-1783OC

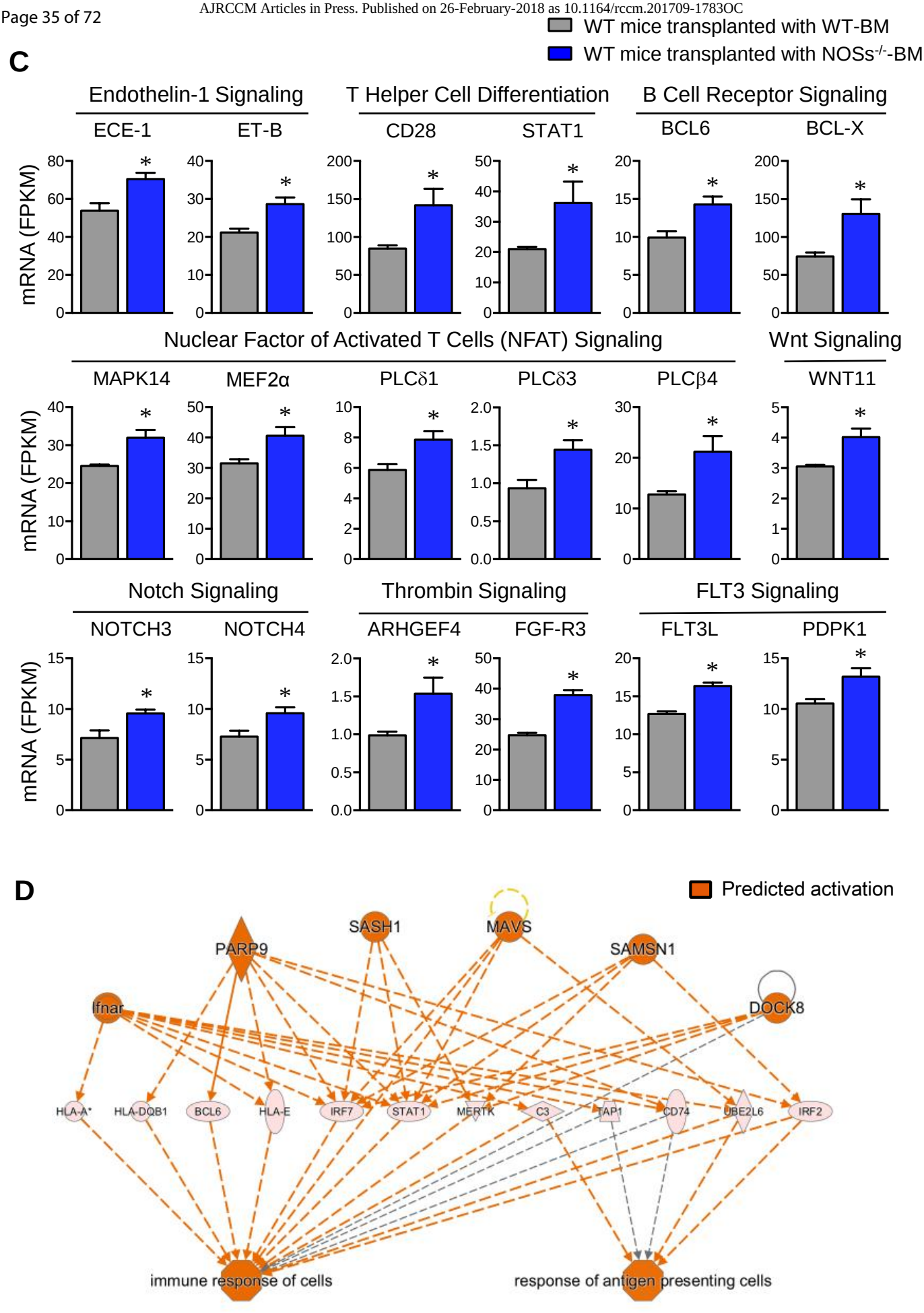

Figure 6 C,D

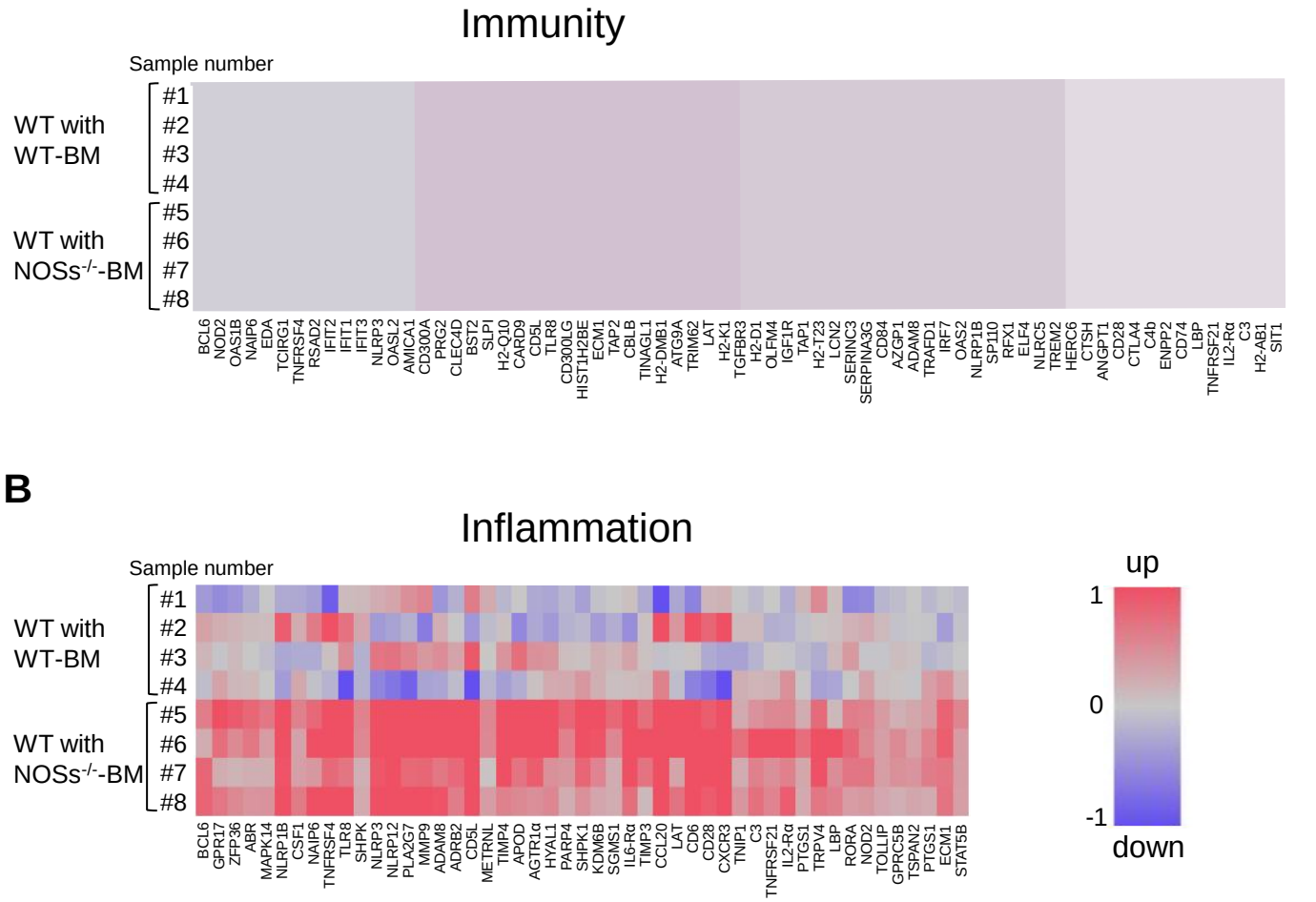

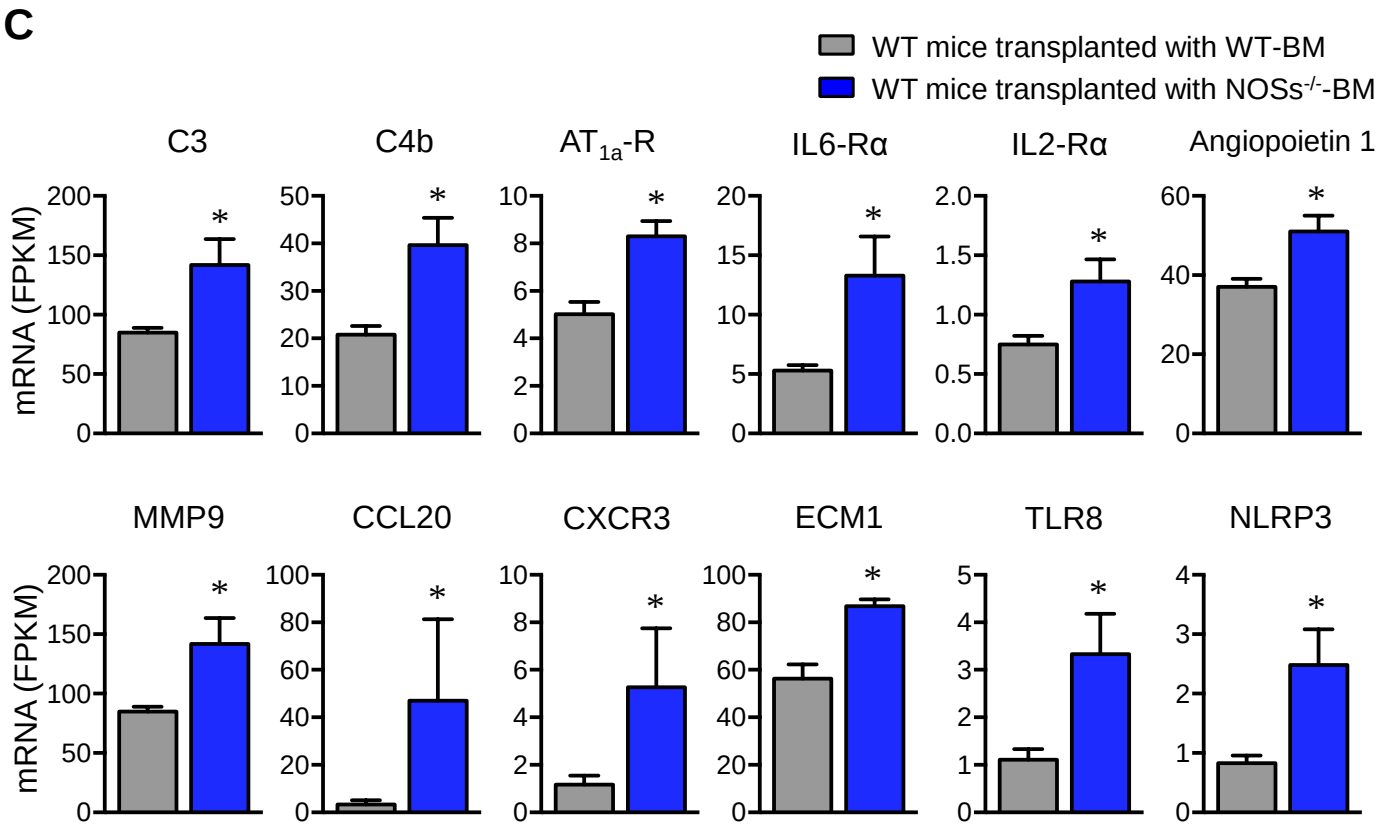

Figure 7 A-C

AJRCCM Articles in Press. Published on 26-February-2018 as 10.1164/rccm.201709-1783OC

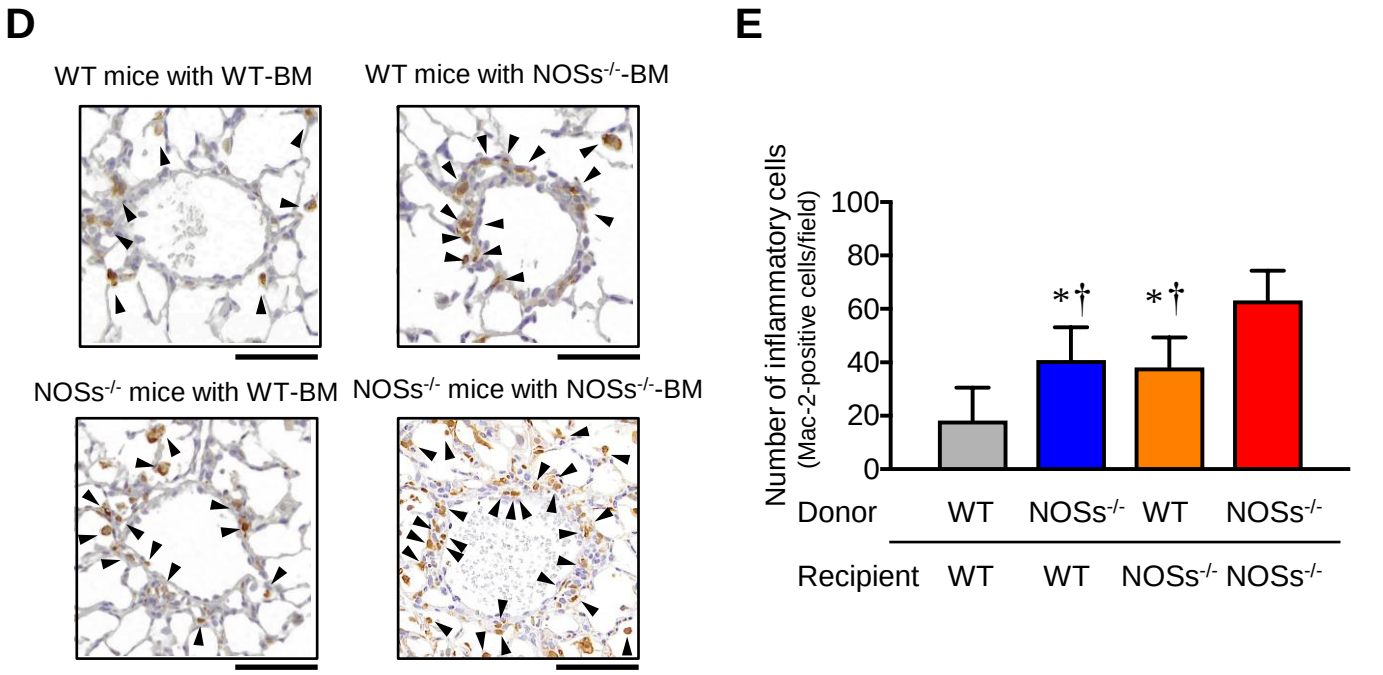

Figure 7 D,E

Supplementary Methods

Subjects

This study was approved by the Institutional Review Board of the University of Occupational and Environmental Health, Japan. As a policy of our department, patients who are suspected to suffer from institutional lung diseases are routinely admitted to our university hospital, and we perform several examinations, including bronchoalveolar lavage fluid (BALF) collection and Doppler echocardiography, in order to determine a diagnosis. We instructed current smokers to refrain from smoking for 2 weeks before the examinations in order to avoid the influence of current smoking on the examinations. Making diagnoses of idiopathic pulmonary fibrosis (IPF) retrospectively according to the official ATS/ERS/JRS/ALAT statement (1), we diagnosed 42 subjects as having idiopathic pulmonary fibrosis between January 2010 and September 2014. We excluded patients who had cardiovascular risk factors (hypertension, hyperlipidemia, diabetes mellitus, and obesity) and who were taking certain medications (nitrates, statins, angiotensin-converting enzyme inhibitors, angiotensin receptor blockers, and cyclooxygenase 2 inhibitors) because such factors and medications can affect systemic NOx levels. Finally, 36 consecutive patients with IPF were studied. All the IPF patients were in stable condition, and no apparent infectious or inflammatory disease was seen.

Pulmonary Arterial Systolic Pressure Measured by Echocardiography

The patients underwent two-dimensional echocardiography with Doppler and color flow imaging. Right atrial pressure was estimated on the basis of inferior vena cava size and movement on respiration (2, 3). Pulmonary arterial systolic pressure was calculated as the sum of the tricuspid peak gradient (based on the modified Bernoulli equation) and the right atrial pressure (4).

Animals

This study was approved by the Ethics Committee of Animal Care and Experimentation, the University of Occupational and Environmental Health, Japan, and was carried out according

AJRCCM Articles in Press. Published on 26-February-2018 as 10.1164/rccm.201709-1783OC

to the Institutional Guidelines for Animal Experimentation. We generated triple n/i/eNOSs$^{-/-}$ mice by crossbreeding each singly NOS$^{-/-}$ mouse (5). Experiments were performed in 8- to 9-week-old male wild-type (WT) C57BL/6J (Kyudo, Co., Ltd., Tosu, Japan), singly nNOS$^{-/-}$, iNOS$^{-/-}$, and eNOS$^{-/-}$, and triple n/i/eNOSs$^{-/-}$ mice and transgenic mice expressing green fluorescent protein (GFP-Tg mice) weighing 20-25g. The mice were maintained on a regular diet (CE-2, CLEA Japan, Inc., Tokyo, Japan). The genotype for the NOS genes was determined by PCR of tail genomic DNA.

Hypoxia Exposure

The mice were housed in sealed acrylic chambers under either normoxia (room air, 21% O_2) or hypoxia (10% O_2) for 3 weeks. The air in the chamber was circulated with a fan, and O_2 concentrations were continuously monitored with an O_2 analyzer (XO-2200, New Cosmos Electric CO., Ltd., Osaka, Japan). Survival of the mice was checked every day, and body weight was measured every 1 week.

BALF Sampling

Sampling of BALF in the IPF patients was carried out by bronchoscopy after overnight fasting (>12 hours), as we previously reported (6). Briefly, the bronchoscope was wedged into the middle lobe bronchus or the lingular lobe bronchus, and bronchoalveolar lavage fluid (BALF) was collected with three instillations of sterile physiological saline (50 mL) through a flexible bronchoscope. The collected BALF was passed through two sheets of gauze, centrifuged at 400×*g* for 10 min at 4 °C, and the supernatant was stored at -80 °C (7). Sampling of BALF in mice was performed by cannulating the trachea with a 20-gauge catheter. The lung was lavaged with three aliquots of 1.5 ml saline (0.9% NaCl). The BALF was centrifuged at 700×*g* for 10 min at 4°C and the supernatants were stored at -80°C. The cell pellet was diluted in PBS, and total cell number was counted with a hemocytometer after staining with Turk's Stain Solution (Merck, Tokyo, Japan). Differential cell counts were determined using the cell suspensions displayed on glass slides using a cytocentrifuge (Cytospin 4; Termo, Kanagawa, Japan). The cells on a slide were dried, fixed and stained

by the Diff-Quick method (Sysmex, Hyogo, Japan), and then three hundred cells were identified under a microscope.

NOx Measurement

NOx (nitrite plus nitrate) concentrations in BALF were assessed by the Griess method with the use of the ENO-20 NOx analysis system (Eicom Co., Ltd., Kyoto, Japan), as we previously reported (5). In mice, the blood samples were collected in vacuum tubes containing sodium EDTA, were immediately centrifuged at 3,000 rpm at 4 °C for 15min, and the supernatant plasma was stored at -80°C. The NOx concentrations in the plasma were also measured by the Griess method (5).

Western blot analysis

Western blot analysis was performed as we previously reported (8). The tissues were homogenized in 0.5 ml of ice-cold homogenization buffer containing 50 mmol/l Tris (pH 8.0), 150 mmol/l NaCl, 0.1% SDS, 20 mmol/l 3-[(3-cholamidepropyl) dimethylammonio]-1-propanesulphonate, and 0.5% protease inhibitor cocktail (Roche, Mannheim, Germany). The tissue homogenates were centrifuged at 15,000 g for 10 min at 4°C, and the supernatants were used for Western blot analysis. To detect neuronal (nNOS), inducible (iNOS), endothelial NO synthase (eNOS), and Arginase-I, 40 μg of the protein were solubilized in a Laemmli sample buffer containing 2.5% 2-mercaptoethanol at 95°C for 5 min, and subjected to 8% SDS-PAGE at room temperature. The gels were transferred to PVDF membranes, and the membranes were blocked with 5% nonfat milk. They were then incubated with antibodies for nNOS (1:1000), iNOS (1:1000), eNOS (1:1000) and Arginase-I (1:1000) (Cell Signaling Technology, Danvers, MA), or anti-glyceraldehyde 3-phosphate dehydrogenase (GAPDH) (1:5000) (Sigma-Aldrich St. Louis, MO) in Tris-buffered saline-Tween. After being washed and incubated with a horseradish peroxidase-conjugated goat anti-rabbit IgG antibody (1:1000) (Cell Signaling Technology), the membranes were developed with an enhanced chemiluminescence system (Western Lightning ECL Pro, PerkinElmer, Waltham, MA). Quantitative densitometry was performed

AJRCCM Articles in Press. Published on 26-February-2018 as 10.1164/rccm.201709-1783OC

by a lumino-image analyser (LAS-4000 mini EPUV; Fuji Film, Japan) and Multi Gauge software (version 3.0).

Hemodynamics

The mice were intubated and anesthetized with 2.0-4.0% sevoflurane at 3 weeks after the exposure to normoxia or hypoxia. They were placed in a supine position and ventilated with normoxic air (21% O_2, 160 breaths per minute, 2 mL tidal volume). The chest was opened by thoracotomy, and a 1.4F micromanometer-tipped catheter was directly inserted into the right ventricle via apical puncture using a slight modification of a previously published technique (9). Right ventricular systolic pressure (RVSP) was measured with a pressure transducer (SPR-671, Millar Instruments, Houston, TX) and the PowerLab data acquisition system (AD Instruments, Colorado Springs, CO). The RVSP was continuously monitored using Chart 7 pro software (AD Instrument, Colorado Springs, CO), and the mean value of RVSP in 15-20 cardiac cycles was used for statistical analysis. Placement of the needle into the right ventricle was confirmed by postmortem examination.

Morphology

The hearts and lungs were quickly dissected after the hemodynamic measurements. The lungs were fixed by intratracheal infusion of 4% phosphate-buffered formalin at a physiological pressure of 23 cmH_2O. The lung sections were immersed in 4% phosphate-buffered formalin, and were stained with a haematoxylin-eosin solution or an elastic van Gieson (EVG) solution. Immunostaining for α-smooth muscle actin (α-SMA), using a monoclonal antibody to anti-α- SMA (clone 1A4, Sigma Aldrich, St. Louis, MO), was also performed, as we previously reported (10). EVG staining is useful for identifying the internal and the external elastic lamina, and vascular smooth muscle cells (VSMCs), and α-SMA staining is useful for specifying VSMCs. Vascular remodeling was evaluated by medial wall thickness in the small pulmonary arteries (50-150 μm in diameter). The vascular cross-sectional area and the vascular lumen area were measured with the Nano Zoomer 2.0 Digital Pathology system (Hamamatsu Photonics Co., Ltd., Shizuoka, Japan) and

their diameters were computed from those data using the formula of the circle area ($=\pi r^2$). The medial wall thickness was expressed as the ratio of the vascular diameter to the medial wall thickness. More than 40 small pulmonary arteries were evaluated in each animal, and the mean value was used for the statistical analysis. Cardiac right ventricular hypertrophy was assessed by the weight ratio of the right ventricle to the left ventricle plus the interventricular septum [RV/(LV+S)] (the Futon index). To evaluate the extent of inflammation in the lung, Mac-2 immunostaining was performed with an anti-mouse Mac-2 monoclonal antibody (1:500; Cedarlane Laboratories Ltd., Burlington, Ontario, Canada) as previously reported (11). These analyses were performed by an experienced pulmonologist in a blind manner.

Treatment with Isosorbide Dinitrate or Sodium Nitrate

Isosorbide dinitrate (ISDN, 0.6 mg/dl, Eisai Co., Ltd., Tokyo, Japan) was dissolved in drinking tap water and administered orally in the triple n/i/eNOS$^{-/-}$ mice from 3 days before the hypoxic exposure to 3 weeks after the hypoxic exposure, as we reported previously (12). Sodium nitrate (Wako Pure Chemical Industries, Osaka, Japan) was dissolved in drinking tap water and administered orally in the triple n/i/eNOS$^{-/-}$ mice from 3 days before to 3 weeks after the hypoxic exposure. We used 2, 5, and 45 mmol/L of sodium nitrate in reference to a previous study (13) and in our thoughts.

Bleomycin Treatment

Bleomycin (8.0 mg/kg/day) was intraperitoneally administered in the WT and triple n/i/eNOSs$^{-/-}$ mice for 10 consecutive days, and PH evaluation was performed at 14 days after the last administration as we previously reported (14).

Bone Marrow-derived Vascular Smooth Muscle Cell Progenitor Cells

Anti-coagulated blood was collected by cardiac puncture under general anesthesia with sodium pentobarbital (50 mg/kg, IP) in order to enumerate circulating bone marrow (BM)-derived vascular smooth muscle cell (VSMC) progenitor cells. After the red blood

AJRCCM Articles in Press. Published on 26-February-2018 as 10.1164/rccm.201709-1783OC

cells were removed by erythrocyte lysis, the peripheral blood cells were incubated with a rat anti-mouse CD16/CD32 monoclonal antibody (mAb) in a staining buffer (magnesium/calcium free phosphate-buffered saline with 1% fetal calf serum and 0.1% sodium azide, pH 7.4) at 4°C for 5 min to block non-specific binding. The cells were then incubated with fluorescein isothiocyanate (FITC)–conjugated lineage markers (Lin^+; CD3, CD11b, CD45R/B220, Ly-6C/G, TER119), with biotin-conjugated mAbs against allophycocyanin (activated protein C [APC])–conjugated Sca-1, and with phycoerythrin (PE)-conjugated c-kit (CD117; all Militeny Biotec, Tokyo, Japan) at 4°C for 40 min in the dark. In addition, for baseline setting, the cells were incubated with an APC mouse lineage isotype control cocktail, with FITC-rat IgG_{2a},κ, and with PE-rat IgG_{2b},κ as a negative control, and the BD CompBeads Compensation particles (BD PharMingen, Tokyo, Japan) were incubated with APC lineage markers, with FITC-Sca-1, and with PE-c-kit as a positive control. At the end, the Sca-1^+/c-kit^+/Lin^- and Sca-1^+/c-kit^-/Lin^- cells were counted with an automated benchtop flow cytometry system (Cell Analyzer EC800, Sony Co., Ltd., Tokyo, Japan), as we previously reported (15).

Stromal Cell-Derived Factor (SDF)-1α

The lung sections were homogenized with 5x volume of PBS plus a protease inhibitor cocktail tablet at 4°C, and the homogenate buffer was centrifuged at 3,000 rpm, 4°C for 5 minutes. Total protein concentrations were determined with a the Bio-Rad protein assay kit (Bio-Rad Laboratories, Hercules, California). SDF-1α levels in the serum and the lung were measured with a commercially available immunoassay kit according to the manufacturer's protocol (R&D Systems, Minneapolis, MN).

BM Transplantation

BM cells were prepared as we previously reported (16). In brief, the donor mice (the WT, $eNOS^{-/-}$, $iNOS^{-/-}$, n/i/$eNOSs^{-/-}$, and GFP-Tg mice) were sacrificed by sodium pentobarbital (50 mg/kg, IP), and the tibias and fibulas were aseptically removed. Fresh BM was pushed out from the bones by using a 25G needle syringe containing 1 ml saline. The dissociated

BM cells were passed through a cell strainer (70 μm nylon, BD Falcon, Bedford, MA), and washed with saline. The recipient WT, eNOS$^{-/-}$, iNOS$^{-/-}$, or n/i/eNOSs$^{-/-}$ mice were subjected to lethal irradiation (9.6 Gy) in order to destroy their BM. On the next day, BM obtained from the WT, eNOS$^{-/-}$, iNOS$^{-/-}$, n/i/eNOSs$^{-/-}$, and GFP-Tg mice was transplanted into the irradiated WT, eNOS$^{-/-}$, iNOS$^{-/-}$, or n/i/eNOSs$^{-/-}$ recipients by tail vein injection. Four weeks after the transplantation, the chimeric mice were kept in hypoxic chambers for 3 weeks.

Fluorescent Staining

The lung sections were freshly embedded in an O.C.T. compound (Sakura Finetek Japan Co., Ltd., Tokyo, Japan), were frozen in liquid acetone at -80°C for 30 seconds using the HistoTek Pino system (Sakura Finetek Japan Co., Ltd., Tokyo, Japan), and were transferred to cryostat using the Tissue-Tek Polar (Sakura Finetek Japan Co., Ltd., Tokyo, Japan). Seven μm-thick sections were stained with an anti-α-SMA antibody (specific for smooth muscle cells) (clone 1A4; Sigma Aldrich; St. Louis, MO) or an anti-4',6-diamidino-2-phenylindole dihydrochloride (DAPI) antibody (specific for the nuclei of cells) (Molecular Probes, Eugene, OR) at 4°C for 30 minutes, and were incubated with a secondary antibody that had been conjugated (Alexa 594, Molecular Probes) at 4°C for 30 minutes. Immunofluorescence was analyzed by confocal laser scanning microscopy with appropriate emission filters. Ten different sections from each animal were evaluated by an experienced pulmonologist in a blind manner, and the mean value was used for the statistical analysis.

Micro Computed Tomographic (CT) Analysis

A contrast medium (150 μl/25 g mouse) (ExiTronTM nano 12000, ViscoverTM, Miltenyi Biotec, Bergisch-Gladbach, Germany) was injected into the mice through the tail vein 1 hour before micro CT analysis. The mice were anesthetized with 2% sevoflurane, and an X-ray micro CT system (Cosmoscan GX, RIGAKU, Tokyo, Japan) was operated under the following conditions: 90 kV, 88 μA, either respiratory or cardiac reconstruction mode in chest

AJRCCM Articles in Press. Published on 26-February-2018 as 10.1164/rccm.201709-1783OC

CT, 24×19 mm view field, and 9×9 μm pixel size. Image segmentation was performed semi-automatically using lung volume edit tools (AnalyzeDirect, Overland Park, KS). The end-systolic and end-diastolic volumes of the RV and LV were measured with an Analyze software, and the RV and LV ejection fractions were calculated according to the manufacturer's instructions (http://analyzedirect.com).

RNA Sequencing

The lungs were isolated and quickly immersed in an RNA stabilization reagent (RNase later, QIAGEN, Valencia, CA) at 3 days after hypoxic exposure. They were then homogenized in Qiazol (QIAGEN) with a homogenizer (Power Masher II, Nippi, Tokyo, Japan), and total RNA was extracted from the homogenized mixture with a miRNeasy mini kit (QIAGEN). In 8 individual samples (4 from the lungs of the WT mice with WT-BM transplantation and 4 from the lungs of the WT mice with triple n/i/eNOS$^{-/-}$-BM transplantation), total RNA concentrations were determined by a spectrophotometer (NanoDrop 2000, Thermo Scientific, Wilmington, DE), and the quality of the total RNA samples was assessed by an Agilent 2100 Bioanalyzer (Agilent Technologies, Palo Alto, CA). The RNA integrity number (RIN) in the 8 samples ranged from 7.8 to 8.2. mRNA was extracted with a Dynabeads mRNA Purfication Kit (Thermo,Waltham, MA), and cDNA was generated from 500 ng of mRNA using a PrimeScript Double Strand cDNA Synthesis Kit (Takara Bio, Otsu, Japan). Fifty ng of each cDNA sample was sheared in 200-500 bp using a Covaris S220 (Covaris, Woburn, MA), and 75 bp single-end reads were prepared using KAPA Library Preparation Kits (Kapa Biosystems, Wilmington, MA). The cDNA libraries were indexed for multiplexing, and were sequenced on an Illumina HiSeq 2500 platform. CASAVA software (v1.8.2, Illumina, San Diego, CA) was used to generate FASTQ-files. The trimmed reads were mapped onto the reference mouse genome mm10 using TopHat program (v2.0.13) in combination with Bowtie2 (v2.2.3) and SAMtools (v0.1.19). Gene expression was quantified with the Cufflinks program (v2.2.1). We detected the raw mapped reads and the fragments per kilobase of exon per million mapped fragments (FPKM). We ignored the genes in which raw gene counts were less than 15 in every 8 samples because of the lower reliability of the

data, and analyzed 13,748 mRNAs out of 23,284 mouse mRNAs enrolled in the reference mouse genome mm10 database. The datasets of mRNA sequences were deposited in NCBIs Gene Expression Omnibus (GEO, http://www.ncbi.nlm.nih.gov/geo/) and are accessible through GEO Series accession number GSE92263.

Statistical analyses

Results are expressed as mean ± SEM. Statistical analyses were performed by a two-sided Student's *t*-test, or an analysis of variance (ANOVA) followed by Bonferroni's *post hoc* test for multiple comparisons. Kaplan-Meier survival curves were plotted and compared by the log-rank test. We used Graph Pad Prism Version 7 (Graph Pad Software Inc., San Diego, CA.), Subio Platform (Subio, Kagoshima, Japan), Ingenuity Pathway Analysis (IPA, QIAGEN), and the Database for Annotation, Visualization, and Integrated Discovery (DAVID) (v6.8). A value of $P<0.05$ was considered to be statistically significant.

References

1. Raghu G, Collard HR, Egan JJ, Martinez FJ, Behr J, Brown KK, Colby TV, Cordier JF, Flaherty KR, Lasky JA, Lynch DA, Ryu JH, Swigris JJ, Wells AU, Ancochea J, Bouros D, Carvalho C, Costabel U, Ebina M, Hansell DM, Johkoh T, Kim DS, King TE, Jr., Kondoh Y, Myers J, Muller NL, Nicholson AG, Richeldi L, Selman M, Dudden RF, Griss BS, Protzko SL, Schunemann HJ, Fibrosis AEJACoIP. An official ATS/ERS/JRS/ALAT statement: idiopathic pulmonary fibrosis: evidence-based guidelines for diagnosis and management. *Am J Respir Crit Care Med* 2011; 183: 788-824.
2. Brittain EL, Duncan MS, Chang J, Patterson OV, DuVall SL, Brandt CA, So-Armah KA, Goetz M, Akgun K, Crothers K, Zola C, Kim J, Gibert C, Pisani M, Morris A, Hsue P, Tindle HA, Justice A, Freiberg M. Increased Echocardiographic Pulmonary

AJRCCM Articles in Press. Published on 26-February-2018 as 10.1164/rccm.201709-1783OC

Pressure in HIV-infected and Uninfected Individuals in the Veterans Aging Cohort Study. *Am J Respir Crit Care Med* 2017.

3. Kircher BJ, Himelman RB, Schiller NB. Noninvasive estimation of right atrial pressure from the inspiratory collapse of the inferior vena cava. *Am J Cardiol* 1990; 66: 493-496.
4. Currie PJ, Seward JB, Chan KL, Fyfe DA, Hagler DJ, Mair DD, Reeder GS, Nishimura RA, Tajik AJ. Continuous wave Doppler determination of right ventricular pressure: a simultaneous Doppler-catheterization study in 127 patients. *J Am Coll Cardiol* 1985; 6: 750-756.
5. Morishita T, Tsutsui M, Shimokawa H, Sabanai K, Tasaki H, Suda O, Nakata S, Tanimoto A, Wang KY, Ueta Y, Sasaguri Y, Nakashima Y, Yanagihara N. Nephrogenic diabetes insipidus in mice lacking all nitric oxide synthase isoforms. *Proc Natl Acad Sci U S A* 2005; 102: 10616-10621.
6. Sakamoto N, Mukae H, Fujii T, Kakugawa T, Kaida H, Kadota J, Kohno S. Soluble form of Fas and Fas ligand in serum and bronchoalveolar lavage fluid of individuals infected with human T-lymphotropic virus type 1. *Respir Med* 2004; 98: 213-219.
7. Sakamoto N, Kakugawa T, Hara A, Nakashima S, Yura H, Harada T, Ishimoto H, Yatera K, Kuwatsuka Y, Hara T, Ichinose K, Obase Y, Ishimatsu Y, Kohno S, Mukae H. Association of elevated alpha-defensin levels with interstitial pneumonia in patients with systemic sclerosis. *Respir Res* 2015; 16: 148.
8. Kina-Tanada M, Sakanashi M, Tanimoto A, Kaname T, Matsuzaki T, Noguchi K, Uchida T, Nakasone J, Kozuka C, Ishida M, Kubota H, Taira Y, Totsuka Y, Kina SI, Sunakawa H, Omura J, Satoh K, Shimokawa H, Yanagihara N, Maeda S, Ohya Y, Matsushita M, Masuzaki H, Arasaki A, Tsutsui M. Long-term dietary nitrite and nitrate deficiency causes the metabolic syndrome, endothelial dysfunction and cardiovascular death in mice. *Diabetologia* 2017; 60: 1138-1151.
9. Pacher P, Nagayama T, Mukhopadhyay P, Batkai S, Kass DA. Measurement of cardiac function using pressure-volume conductance catheter technique in mice and rats. *Nat Protoc* 2008; 3: 1422-1434.

10. Morisada N, Nomura M, Nishii H, Furuno Y, Sakanashi M, Sabanai K, Toyohira Y, Ueno S, Watanabe S, Tamura M, Matsumoto T, Tanimoto A, Sasaguri Y, Shimokawa H, Kusuhara K, Yanagihara N, Shirahata A, Tsutsui M. Complete disruption of all nitric oxide synthase genes causes markedly accelerated renal lesion formation following unilateral ureteral obstruction in mice in vivo. *J Pharmacol Sci* 2010; 114: 379-389.

11. Noguchi H, Yamada S, Nabeshima A, Guo X, Tanimoto A, Wang KY, Kitada S, Tasaki T, Takama T, Shimajiri S, Horlad H, Komohara Y, Izumi H, Kohno K, Ichijo H, Sasaguri Y. Depletion of apoptosis signal-regulating kinase 1 prevents bile duct ligation-induced necroinflammation and subsequent peribiliary fibrosis. *Am J Pathol* 2014; 184: 644-661.

12. Furuno Y, Morishita T, Toyohira Y, Yamada S, Ueno S, Morisada N, Sugita K, Noguchi K, Sakanashi M, Miyata H, Tanimoto A, Sasaguri Y, Shimokawa H, Otsuji Y, Yanagihara N, Tamura M, Tsutsui M. Crucial vasculoprotective role of the whole nitric oxide synthase system in vascular lesion formation in mice: Involvement of bone marrow-derived cells. *Nitric Oxide* 2011; 25: 350-359.

13. Baliga RS, Milsom AB, Ghosh SM, Trinder SL, Macallister RJ, Ahluwalia A, Hobbs AJ. Dietary nitrate ameliorates pulmonary hypertension: cytoprotective role for endothelial nitric oxide synthase and xanthine oxidoreductase. *Circulation* 2012; 125: 2922-2932.

14. Noguchi S, Yatera K, Wang KY, Oda K, Akata K, Yamasaki K, Kawanami T, Ishimoto H, Toyohira Y, Shimokawa H, Yanagihara N, Tsutsui M, Mukae H. Nitric oxide exerts protective effects against bleomycin-induced pulmonary fibrosis in mice. *Respir Res* 2014; 15: 92.

15. Uchida T, Furuno Y, Tanimoto A, Toyohira Y, Arakaki K, Kina-Tanada M, Kubota H, Sakanashi M, Matsuzaki T, Noguchi K, Nakasone J, Igarashi T, Ueno S, Matsushita M, Ishiuchi S, Masuzaki H, Ohya Y, Yanagihara N, Shimokawa H, Otsuji Y, Tamura M, Tsutsui M. Development of an experimentally useful model of acute myocardial infarction: 2/3 nephrectomized triple nitric oxide synthases-deficient mouse. *J Mol*

AJRCCM Articles in Press. Published on 26-February-2018 as 10.1164/rccm.201709-1783OC

Cell Cardiol 2014; 77: 29-41.

16. Sasaguri Y, Wang KY, Tanimoto A, Tsutsui M, Ueno H, Murata Y, Kohno Y, Yamada S, Ohtsu H. Role of histamine produced by bone marrow-derived vascular cells in pathogenesis of atherosclerosis. *Circ Res* 2005; 96: 974-981.

Supplementary Figure E1

No significant correlations between NOx, nitrate, or nitrite levels in BALF and cellular profile in BALF, lung function, serum KL-6 or LDH levels, or arterial oxygenation levels in patients with idiopathic pulmonary fibrosis. (**A-E**) Correlations between NOx, nitrate, or nitrite levels in BALF and total cell counts, ratio of neutrophils, lymphocytes, or eosinophils, or CD4/8 lymphocyte subset ratio in BALF. (**F**) Correlations between NOx, nitrate, or nitrite levels in BALF and % FVC (% forced vital capacity). (**G**) Correlations between NOx, nitrate, or nitrite levels in BALF and %DLCO (% diffusing capacity of the lung carbon monoxide). (**H,I**) Correlations between NOx, nitrate, or nitrite levels in BALF and serum Krebs von den Lungen-6 (KL-6) or lactate dehydrogenase (LDH) levels. (**J**) Correlations between NOx, nitrate, or nitrite levels in BALF and PaO_2 (partial pressure of oxygen in arterial blood.

Supplementary Figure E2

Body weight in WT, single NOS$^{-/-}$, and triple n/i/eNOSs$^{-/-}$ mice exposed to normoxia or hypoxia. **P*<0.05 vs. WT mice (n=19-34).

Supplementary Figure E3

Arginase-1 protein levels in lung in WT, single NOS$^{-/-}$, and triple n/i/eNOSs$^{-/-}$ mice exposed to normoxia or hypoxia. (**A, B**) Arginase-1 levels in the lung after the normoxic and hypoxic exposure (n=4-5). **P*<0.05 vs. normoxia.

Supplementary Figure E4

Effects of a NO donor on survival rate, body weight, plasma NOx levels, and hypoxia-induced PH in n/i/eNOSs$^{-/-}$ mice. Isosorbide dinitrate (ISDN, 0.6 mg/dl) in drinking water was administered orally to the n/i/eNOSs$^{-/-}$ mice from 3 days before to 3 weeks after the hypoxic exposure. (**A**) Survival rate (n=19-34). (**B**) Body weight (n=19-34). (**C**) Plasma NOx levels (n=5-10). (**D-F**) Hypoxia-induced PH (n=5-10). **P*<0.05 vs. without ISDN.

AJRCCM Articles in Press. Published on 26-February-2018 as 10.1164/rccm.201709-1783OC

Supplementary Figure E5

Effects of sodium nitrate on survival rate, body weight, plasma NOx levels, and hypoxia-induced PH in n/i/eNOSs$^{-/-}$ mice. Sodium nitrate (2, 5, and 45 mmol/L) in drinking water was administered orally to the n/i/eNOSs$^{-/-}$ mice from 3 days before to 3 weeks after the hypoxic exposure. **(A)** Survival rate (n=18-34). **(B)** Body weight (n=18-34). **(C)** Plasma NOx levels (n=6-10). **(D-F)** Hypoxia-induced PH (n=6-10). **P*<0.05 vs. without sodium nitrate.

Supplementary Figure E6

Bleomycin-induced PH in WT or n/i/eNOSs$^{-/-}$ mice. **(A, B)** RVSP and RV/(LV+S) after bleomycin treatment (n=6-8). **(C)** H&E, elastic van Gieson (EVG), and α-smooth muscle actin (α-SMA) staining of the small pulmonary arteries. Scale bar=50 μm. **(D)** Medial thickness of the small pulmonary arteries (n=6-8). **P*<0.05 vs. WT.

Supplementary Figure E7

Plasma NOx levels and hypoxia-induced PH in WT and eNOS$^{-/-}$ mice transplanted with either WT-BM or eNOS$^{-/-}$-BM. (**A**) Plasma NOx levels (n=4-6). (**B-D**) Hypoxia-induced PH (n=4-6). **P*<0.05 vs. WT mice transplanted with WT-BM.

Supplementary Figure E8

Plasma NOx levels and hypoxia-induced PH in WT and iNOS$^{-/-}$ mice transplanted with either WT-BM or iNOS$^{-/-}$-BM. (**A**) Plasma NOx levels (n=5-6). (**B-D**) Hypoxia-induced PH (n=5-6). **P*<0.05 vs. WT mice transplanted with WT-BM.

Supplementary Figure E9

Schematic work-flow in analysis of gene lists generated from the transcriptome profiling experiments. Gene lists represent gene products significantly up-regulated and down-regulated in the lungs of WT mice transplanted with n/i/eNOSs$^{-/-}$-BM as compared with those with WT-BM after the hypoxic exposure (*P*<0.05, fold change >1.2, n=4 each).

Lists of differentially expressed genes were analyzed by two types of software: the software of database for annotation, visualization, and integrated discovery (DAVID) and the software of ingenuity pathways analysis (IPA). Important representative genes were also manually picked up. GO, gene ontology

AJRCCM Articles in Press. Published on 26-February-2018 as 10.1164/rccm.201709-1783OC

Supplementary Table E1

Baseline characteristics of patients with idiopathic pulmonary fibrosis at the time of diagnosis.

Parameters	Total (n=36)	
Observation period (days)	926	(627-1396)
Gender		
Male/Female	23/13	(63.9/36.1)
Age (years)	71.0	(63.5-75.0)
Smoking status		
Never/Former/Current	10/17/9	(27.8/47.2/25.0)
BMI	23.0	(20.5-25.9)
mMRC (≥2)	13	(36.1)
FVC (% predicted)	69.0	(54.5-85.5)
DLCO (% predicted) (n=30)	58.5	(44.0-74.0)
Cell analysis of BALF		
Total cell count, median $\times 10^5$/mL	2.17	(1.43-3.10)
Neutrophil (%)	5.33	(2.83-11.9)
Lymphocyte (%)	5.31	(3.19-15.5)
Eosinophil (%)	3.84	(2.23-6.62)
CD4/8 ratio	1.37	(1.20-1.75)
NOx analysis of BALF		
BALF NOx (nM)	178	(122-308)
BALF nitrate (nM)	174	(117-307)
BALF nitrite (nM)	2.13	(1.23-3.52)
Serum KL-6 (U/mL)	997	(732-1544)
Serum LDH (U/L)	232	(203-255)
PaO_2 (mmHg)	77.5	(68.5-87.0)
PAP (mmHg)	36.0	(30.9-40.7)

Each parameter is expressed as number (percentage) or median (interquartile range). Abbreviations: BMI, body mass index; mMRC, modified medical research council; PaO_2, partial pressure of oxygen in arterial blood; FVC, forced vital capacity; DLCO, diffusing capacity of the lung carbon monoxide; BALF, bronchoalveolar lavage fluid; CD4/8, CD4/8 lymphocyte subset ratio; NOx, nitrite plus nitrate; KL-6, Krebs von den Lungen-6; LDH, lactate dehydrogenase; PAP, pulmonary artery systolic pressures

AJRCCM Articles in Press. Published on 26-February-2018 as 10.1164/rccm.201709-1783OC

Supplementary Table E2

Statistically significant biological process terms detected by gene ontology (GO) analysis by the software of database for annotation, visualization, and integrated discovery (DAVID) in up-regulated genes in the lungs of WT mice transplanted with triply n/i/eNOSs$^{-/-}$-BM as compared with those with WT-BM after the hypoxic exposure (P<0.05, fold change >1.2, n=4 each).

GO Term		P value
GO:0002376	immune system process	1.37E-10
GO:0006629	lipid metabolic process	4.24E-07
GO:0072332	intrinsic apoptotic signaling pathway by p53 class mediator	1.02E-05
GO:0002485	antigen processing and presentation of endogenous peptide antigen via MHC class I via ER pathway, TAP-dependent	2.73E-05
GO:0009615	response to virus	5.11E-05
GO:0006955	immune response	9.71E-05
GO:0008152	metabolic process	1.63E-04
GO:0019915	lipid storage	2.83E-04
GO:0045087	innate immune response	3.16E-04
GO:0002489	antigen processing and presentation of endogenous peptide antigen via MHC class Ib via ER pathway, TAP-dependent	3.19E-04
GO:0001525	angiogenesis	3.97E-04
GO:0006914	autophagy	5.09E-04
GO:0055072	iron ion homeostasis	5.40E-04
GO:0048821	erythrocyte development	6.07E-04
GO:0030048	actin filament-based movement	7.13E-04
GO:0002474	antigen processing and presentation of peptide antigen via MHC class I	8.28E-04
GO:0045860	positive regulation of protein kinase activity	1.00E-03
GO:0006954	inflammatory response	0.00107
GO:0051607	defense response to virus	0.00115
GO:0017144	drug metabolic process	0.00129
GO:0035556	intracellular signal transduction	0.00134

GO:0070588	calcium ion transmembrane transport	0.00197
GO:0006006	glucose metabolic process	0.00242
GO:0042771	intrinsic apoptotic signaling pathway in response to DNA damage by p53 class mediator	0.00268
GO:0006816	calcium ion transport	0.00284
GO:0000045	autophagosome assembly	0.00312
GO:0043030	regulation of macrophage activation	0.00336
GO:0002591	positive regulation of antigen processing and presentation of peptide antigen via MHC class I	0.00336
GO:0010875	positive regulation of cholesterol efflux	0.00361
GO:0043410	positive regulation of MAPK cascade	0.00421
GO:0006919	activation of cysteine-type endopeptidase activity involved in apoptotic process	0.00510
GO:0043065	positive regulation of apoptotic process	0.00698
GO:0016310	phosphorylation	0.00726
GO:0050731	positive regulation of peptidyl-tyrosine phosphorylation	0.00738
GO:0033138	positive regulation of peptidyl-serine phosphorylation	0.00743
GO:0035457	cellular response to interferon-alpha	0.00749
GO:0090181	regulation of cholesterol metabolic process	0.00749
GO:0002481	antigen processing and presentation of exogenous protein antigen via MHC class Ib, TAP-dependent	0.00749
GO:0051127	positive regulation of actin nucleation	0.00749
GO:0071456	cellular response to hypoxia	0.00773
GO:0008203	cholesterol metabolic process	0.00883
GO:1900026	positive regulation of substrate adhesion-dependent cell spreading	0.00994
GO:0030278	regulation of ossification	0.01155
GO:0007420	brain development	0.01180
GO:0005975	carbohydrate metabolic process	0.01196
GO:0001934	positive regulation of protein phosphorylation	0.01211
GO:0006811	ion transport	0.01212
GO:0032868	response to insulin	0.01297
GO:0006382	adenosine to inosine editing	0.01300
GO:0097190	apoptotic signaling pathway	0.01303
GO:0035458	cellular response to interferon-beta	0.01333
GO:0006805	xenobiotic metabolic process	0.01390

AJRCCM Articles in Press. Published on 26-February-2018 as 10.1164/rccm.201709-1783OC

GO:0043066	negative regulation of apoptotic process	0.01403
GO:0006631	fatty acid metabolic process	0.01419
GO:0000165	MAPK cascade	0.01472
GO:0001666	response to hypoxia	0.01479
GO:0006869	lipid transport	0.01482
GO:0000422	mitophagy	0.01528
GO:0045785	positive regulation of cell adhesion	0.01580
GO:0051497	negative regulation of stress fiber assembly	0.01653
GO:0019432	triglyceride biosynthetic process	0.01761
GO:0007155	cell adhesion	0.01777
GO:0007219	Notch signaling pathway	0.01785
GO:0043154	negative regulation of cysteine-type endopeptidase activity involved in apoptotic process	0.01880
GO:0001701	in utero embryonic development	0.01918
GO:0007178	transmembrane receptor protein serine/threonine kinase signaling pathway	0.01946
GO:0006928	movement of cell or subcellular component	0.01946
GO:0001946	lymphangiogenesis	0.02209
GO:0043691	reverse cholesterol transport	0.02209
GO:0008217	regulation of blood pressure	0.02254
GO:0050766	positive regulation of phagocytosis	0.02434
GO:0045766	positive regulation of angiogenesis	0.02533
GO:0072661	protein targeting to plasma membrane	0.02621
GO:0016055	Wnt signaling pathway	0.02630
GO:0032496	response to lipopolysaccharide	0.02671
GO:0042593	glucose homeostasis	0.02677
GO:0019886	antigen processing and presentation of exogenous peptide antigen via MHC class II	0.02713
GO:0001921	positive regulation of receptor recycling	0.02713
GO:0043434	response to peptide hormone	0.02786
GO:0060742	epithelial cell differentiation involved in prostate gland development	0.03047
GO:0060315	negative regulation of ryanodine-sensitive calcium-release channel activity	0.03047
GO:0045602	negative regulation of endothelial cell differentiation	0.03047
GO:0042270	protection from natural killer cell mediated cytotoxicity	0.03047
GO:0042493	response to drug	0.03106

GO:0055114	oxidation-reduction process	0.03320
GO:0051092	positive regulation of NF-kappaB transcription factor activity	0.03322
GO:0090200	positive regulation of release of cytochrome c from mitochondria	0.03420
GO:0033344	cholesterol efflux	0.03420
GO:0042130	negative regulation of T cell proliferation	0.03432
GO:0006468	protein phosphorylation	0.03556
GO:0009636	response to toxic substance	0.03779
GO:0051402	neuron apoptotic process	0.03786
GO:0015758	glucose transport	0.03867
GO:0035023	regulation of Rho protein signal transduction	0.03870
GO:0006790	sulfur compound metabolic process	0.03888
GO:0008202	steroid metabolic process	0.04066
GO:0019882	antigen processing and presentation	0.04095
GO:0006013	mannose metabolic process	0.04131
GO:0002830	positive regulation of type 2 immune response	0.04131
GO:0042308	negative regulation of protein import into nucleus	0.04131
GO:0006739	NADP metabolic process	0.04131
GO:0010890	positive regulation of sequestering of triglyceride	0.04131
GO:0019722	calcium-mediated signaling	0.04162
GO:0001974	blood vessel remodeling	0.04162
GO:0071479	cellular response to ionizing radiation	0.04346
GO:0010977	negative regulation of neuron projection development	0.04427
GO:0006810	transport	0.04452
GO:0030890	positive regulation of B cell proliferation	0.04560
GO:0007623	circadian rhythm	0.04560
GO:0001933	negative regulation of protein phosphorylation	0.04593
GO:0071773	cellular response to BMP stimulus	0.04856
GO:0050728	negative regulation of inflammatory response	0.04872

AJRCCM Articles in Press. Published on 26-February-2018 as 10.1164/rccm.201709-1783OC

Supplementary Table E3

Statistically significant terms in the biological process detected by GO analysis by the DAVID software in down-regulated genes in the lungs of WT mice transplanted with triply n/i/eNOSs$^{-/-}$-BM as compared with those with WT-BM after hypoxic exposure (*P*<0.05, fold change >1.2, n=4 each).

GO Term		*P* Value
GO:0006457	protein folding	1.85E-14
GO:0006412	translation	7.33E-11
GO:0006281	DNA repair	3.94E-09
GO:0006260	DNA replication	2.72E-08
GO:0032543	mitochondrial translation	6.12E-07
GO:0042254	ribosome biogenesis	4.89E-06
GO:0006397	mRNA processing	5.54E-06
GO:0006974	cellular response to DNA damage stimulus	6.86E-06
GO:0006364	rRNA processing	9.01E-06
GO:0008380	RNA splicing	9.11E-06
GO:0032259	methylation	9.99E-06
GO:0008033	tRNA processing	1.01E-05
GO:0051028	mRNA transport	1.17E-05
GO:0006303	double-strand break repair via nonhomologous end joining	1.64E-05
GO:0006270	DNA replication initiation	1.64E-05
GO:0016126	sterol biosynthetic process	3.12E-05
GO:0015031	protein transport	5.30E-05
GO:0000387	spliceosomal snRNP assembly	5.79E-05
GO:0045454	cell redox homeostasis	8.60E-05
GO:0006694	steroid biosynthetic process	1.04E-04
GO:0006888	ER to Golgi vesicle-mediated transport	1.16E-04
GO:0071897	DNA biosynthetic process	1.18E-04
GO:0006310	DNA recombination	2.30E-04
GO:0007049	cell cycle	2.53E-04

GO:0006695	cholesterol biosynthetic process	3.91E-04
GO:0006418	tRNA aminoacylation for protein translation	4.06E-04
GO:0016192	vesicle-mediated transport	4.88E-04
GO:0006479	protein methylation	5.08E-04
GO:0000398	mRNA splicing, via spliceosome	5.27E-04
GO:0001649	osteoblast differentiation	5.95E-04
GO:0055114	oxidation-reduction process	6.06E-04
GO:0006268	DNA unwinding involved in DNA replication	6.17E-04
GO:0016446	somatic hypermutation of immunoglobulin genes	0.00114
GO:0034976	response to endoplasmic reticulum stress	0.00141
GO:0051301	cell division	0.00146
GO:0010811	positive regulation of cell-substrate adhesion	0.00167
GO:0061051	positive regulation of cell growth involved in cardiac muscle cell development	0.00199
GO:0006163	purine nucleotide metabolic process	0.00199
GO:0007067	mitotic nuclear division	0.00227
GO:0008299	isoprenoid biosynthetic process	0.00237
GO:0010501	RNA secondary structure unwinding	0.00277
GO:0070126	mitochondrial translational termination	0.00278
GO:0043985	histone H4-R3 methylation	0.00278
GO:0018216	peptidyl-arginine methylation	0.00278
GO:0007017	microtubule-based process	0.00282
GO:0006302	double-strand break repair	0.00299
GO:0061077	chaperone-mediated protein folding	0.00326
GO:0001522	pseudouridine synthesis	0.00326
GO:0006890	retrograde vesicle-mediated transport, Golgi to ER	0.00351
GO:0050821	protein stabilization	0.00410
GO:0006950	response to stress	0.00479
GO:0006606	protein import into nucleus	0.00662
GO:0008202	steroid metabolic process	0.00800
GO:0018279	protein N-linked glycosylation via asparagine	0.00816
GO:0006487	protein N-linked glycosylation	0.00816
GO:0032790	ribosome disassembly	0.00878

AJRCCM Articles in Press. Published on 26-February-2018 as 10.1164/rccm.201709-1783OC

GO:0000413	protein peptidyl-prolyl isomerization	0.00924
GO:0009790	embryo development	0.00959
GO:0006611	protein export from nucleus	0.00981
GO:0016049	cell growth	0.01115
GO:0032092	positive regulation of protein binding	0.01146
GO:0010388	cullin deneddylation	0.01334
GO:0051103	DNA ligation involved in DNA repair	0.01334
GO:0006406	mRNA export from nucleus	0.01378
GO:2000379	positive regulation of reactive oxygen species metabolic process	0.01378
GO:0006284	base-excision repair	0.01378
GO:0008203	cholesterol metabolic process	0.01387
GO:0071353	cellular response to interleukin-4	0.01402
GO:0043968	histone H2A acetylation	0.01555
GO:0032212	positive regulation of telomere maintenance via telomerase	0.01613
GO:0014911	positive regulation of smooth muscle cell migration	0.01658
GO:0043044	ATP-dependent chromatin remodeling	0.01695
GO:0006139	nucleobase-containing compound metabolic process	0.01875
GO:0006241	CTP biosynthetic process	0.01902
GO:0030071	regulation of mitotic metaphase/anaphase transition	0.01902
GO:0000463	maturation of LSU-rRNA from tricistronic rRNA transcript (SSU-rRNA, 5.8S rRNA, LSU-rRNA)	0.01902
GO:0006228	UTP biosynthetic process	0.01902
GO:0006183	GTP biosynthetic process	0.01902
GO:0006413	translational initiation	0.02254
GO:0045740	positive regulation of DNA replication	0.02407
GO:0072593	reactive oxygen species metabolic process	0.02482
GO:0006810	transport	0.02496
GO:1903377	negative regulation of oxidative stress-induced neuron intrinsic apoptotic signaling pathway	0.02500
GO:0019919	peptidyl-arginine methylation, to asymmetrical-dimethyl arginine	0.02500
GO:0006048	UDP-N-acetylglucosamine biosynthetic process	0.02500
GO:0045039	protein import into mitochondrial inner membrane	0.02500
GO:0035246	peptidyl-arginine N-methylation	0.02500

GO:0048254	snoRNA localization	0.02500
GO:0000281	mitotic cytokinesis	0.02803
GO:0002053	positive regulation of mesenchymal cell proliferation	0.02830
GO:0042177	negative regulation of protein catabolic process	0.02830
GO:0042346	positive regulation of NF-kappaB import into nucleus	0.02966
GO:0007131	reciprocal meiotic recombination	0.02966
GO:0006298	mismatch repair	0.02966
GO:0009117	nucleotide metabolic process	0.03255
GO:0032508	DNA duplex unwinding	0.03255
GO:0048660	regulation of smooth muscle cell proliferation	0.03377
GO:0007160	cell-matrix adhesion	0.03408
GO:0010976	positive regulation of neuron projection development	0.03820
GO:0006415	translational termination	0.03982
GO:0000154	rRNA modification	0.03982
GO:0008152	metabolic process	0.04041
GO:0006986	response to unfolded protein	0.04118
GO:0000462	maturation of SSU-rRNA from tricistronic rRNA transcript (SSU-rRNA, 5.8S rRNA, LSU-rRNA)	0.04222
GO:0060044	negative regulation of cardiac muscle cell proliferation	0.04281
GO:0015693	magnesium ion transport	0.04281
GO:0043039	tRNA aminoacylation	0.04281
GO:0008283	cell proliferation	0.04464
GO:0030199	collagen fibril organization	0.04535
GO:0032467	positive regulation of cytokinesis	0.04869

AJRCCM Articles in Press. Published on 26-February-2018 as 10.1164/rccm.201709-1783OC

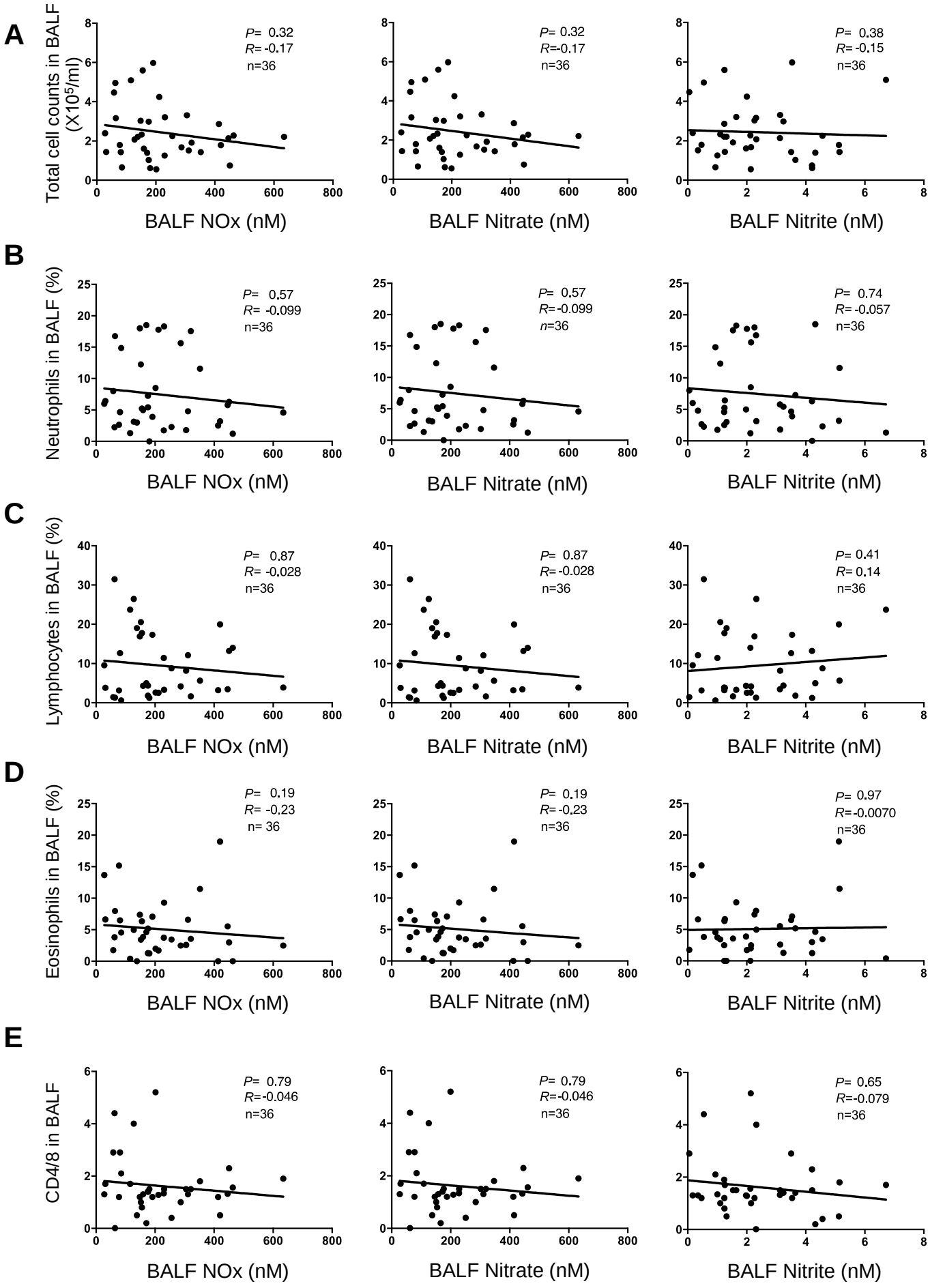

Supplementary Figure E1 A-E

F

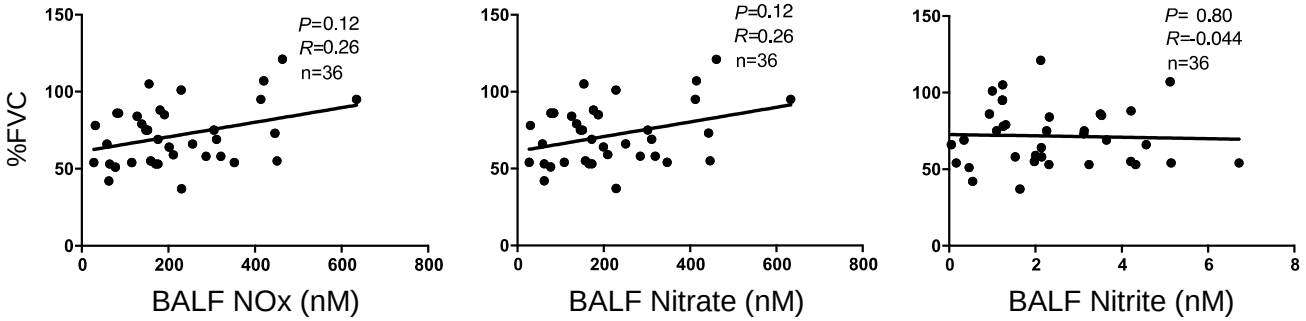

G

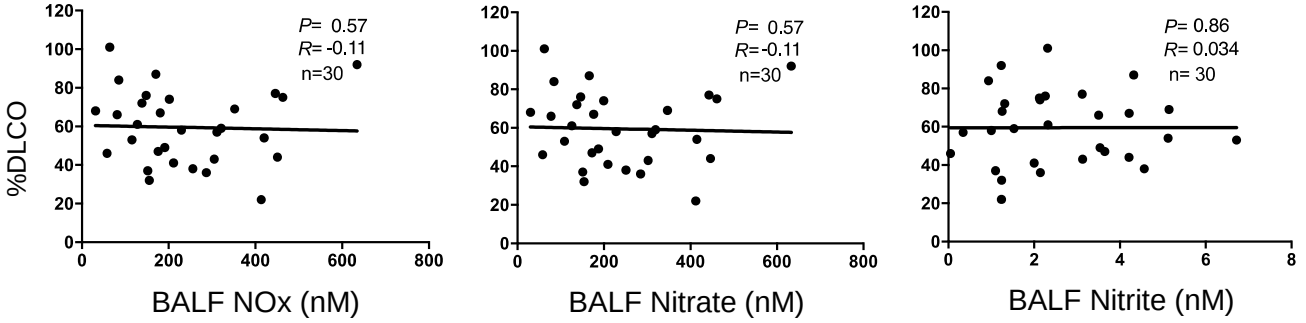

H

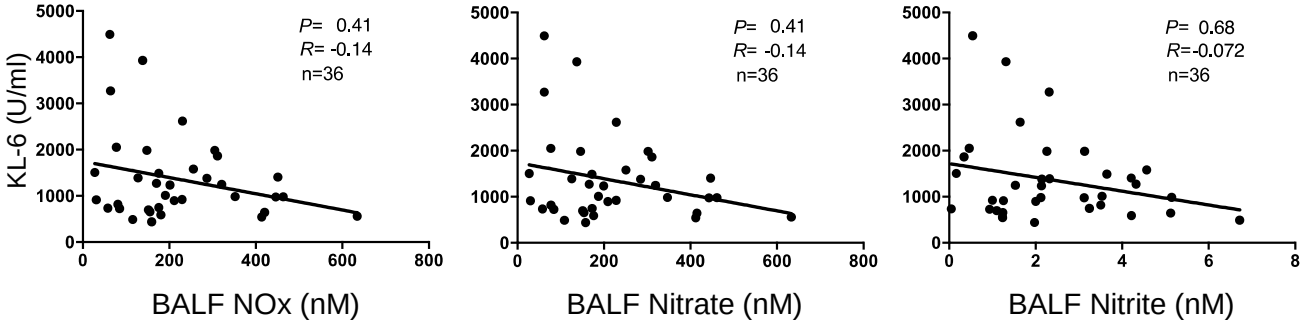

I

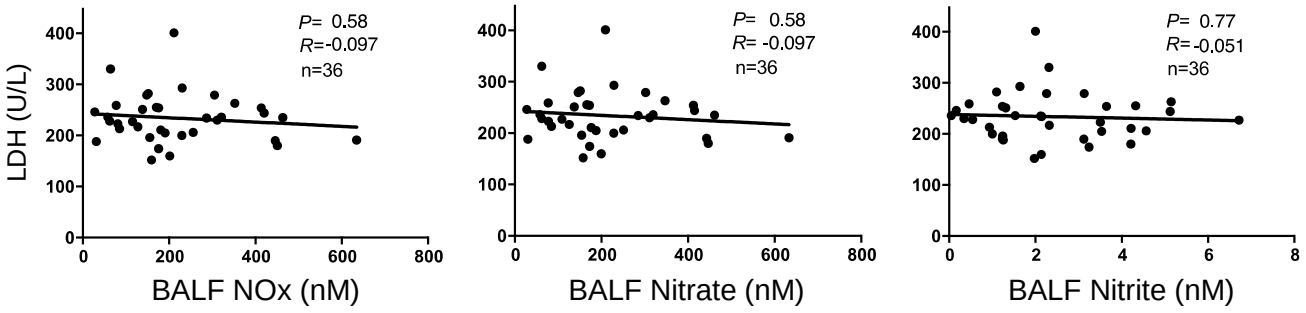

J

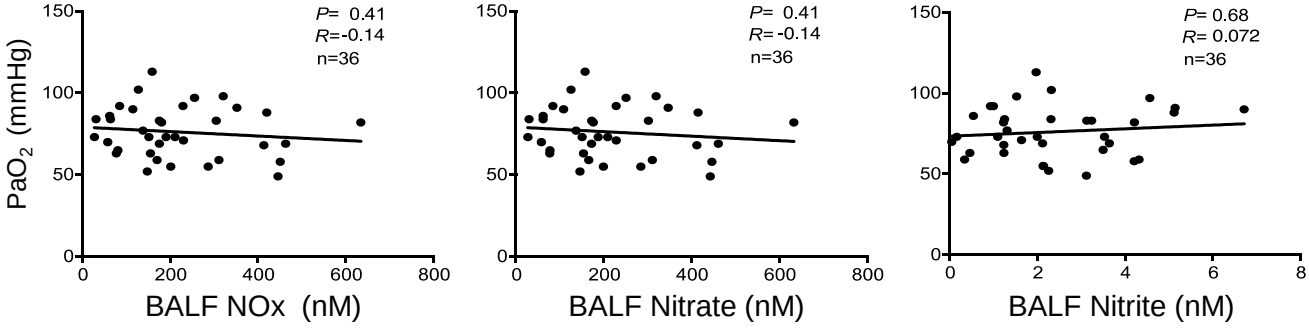

Supplementary Figure E1 F-J

AJRCCM Articles in Press. Published on 26-February-2018 as 10.1164/rccm.201709-1783OC

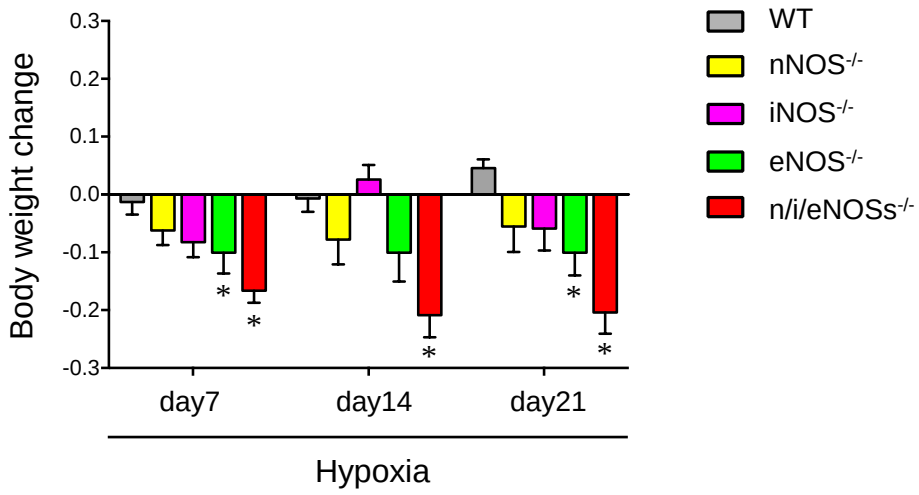

Supplementary Figure E2

A

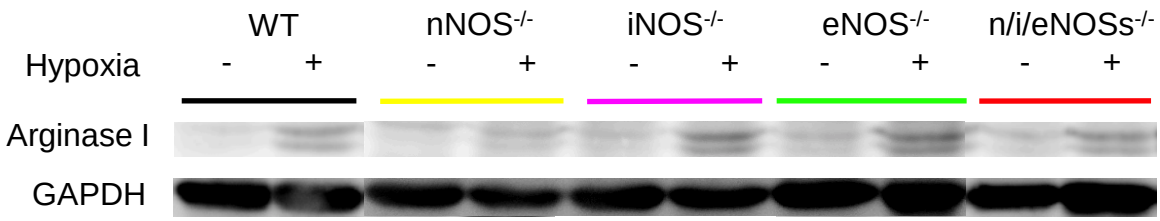

B

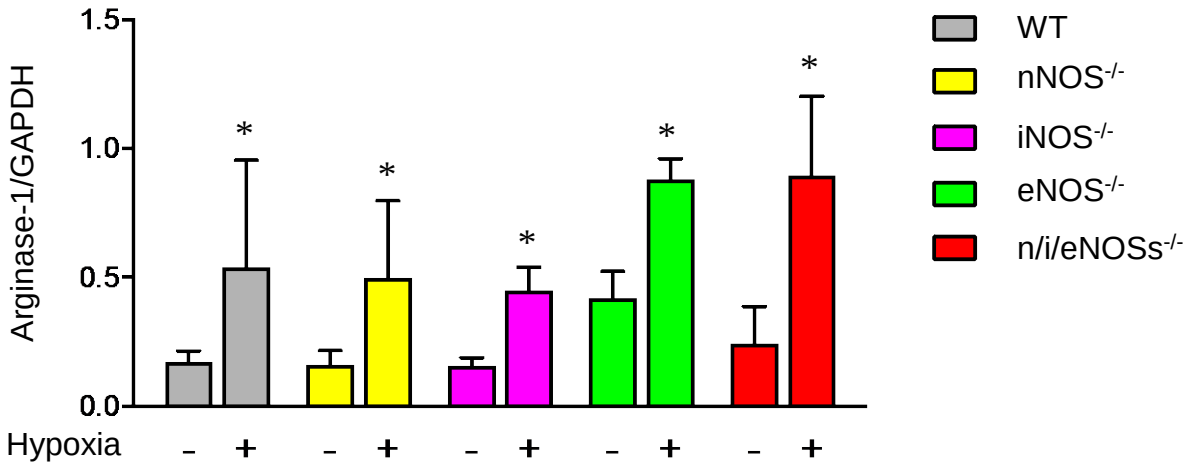

Supplementary Figure E3

AJRCCM Articles in Press. Published on 26-February-2018 as 10.1164/rccm.201709-1783OC

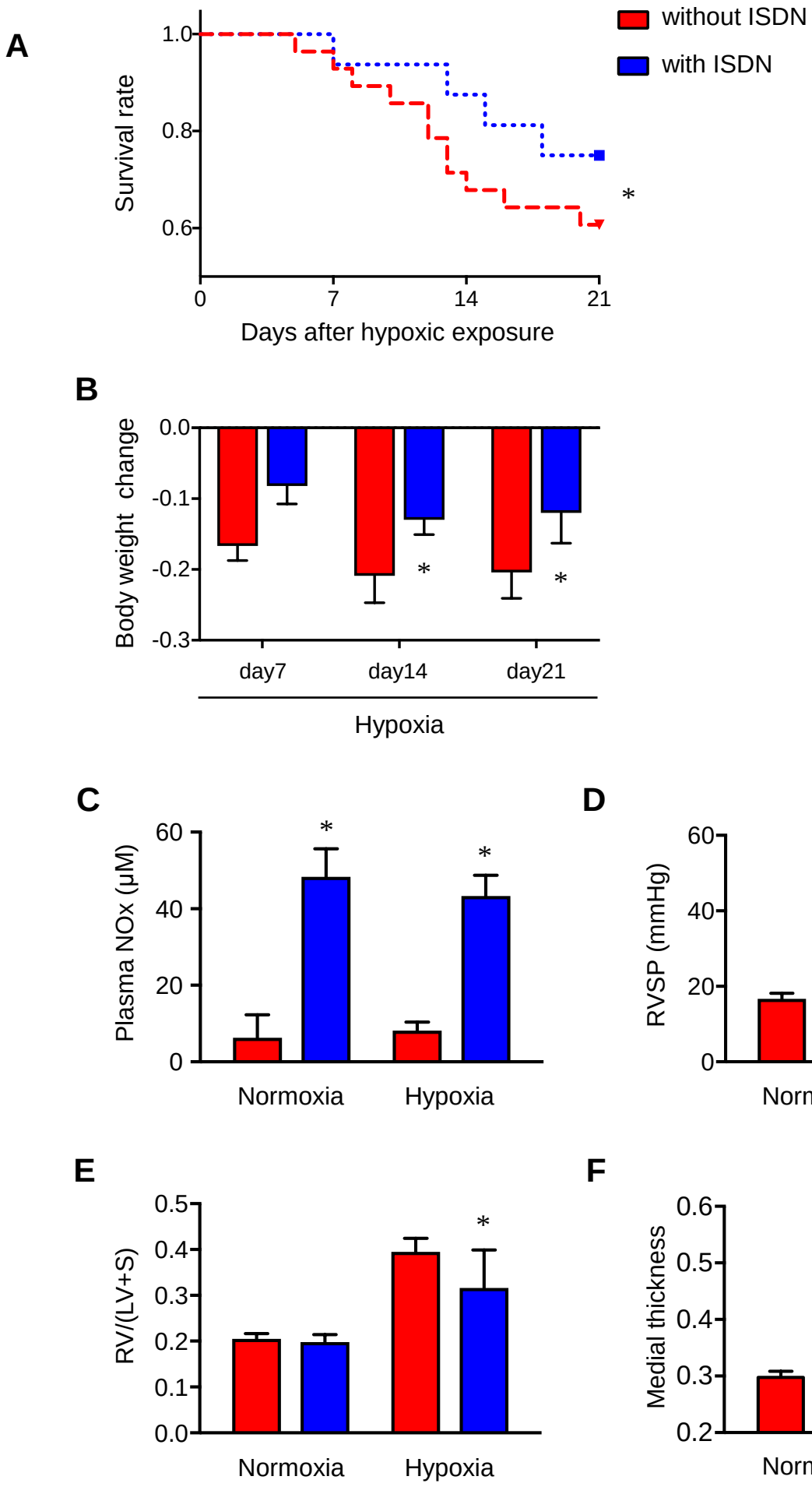

Supplementary Figure E4

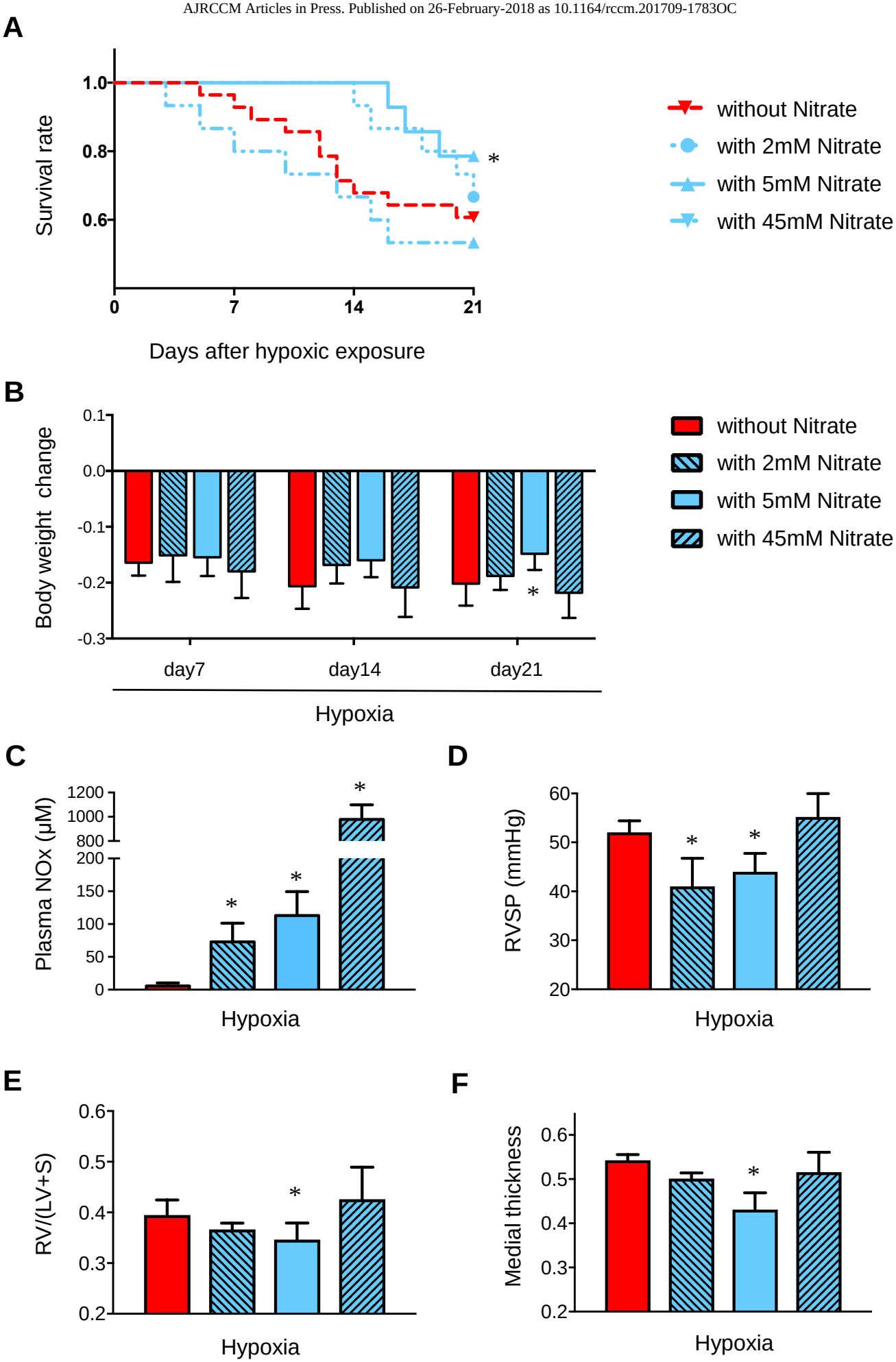

Supplementary Figure E5

AJRCCM Articles in Press. Published on 26-February-2018 as 10.1164/rccm.201709-1783OC

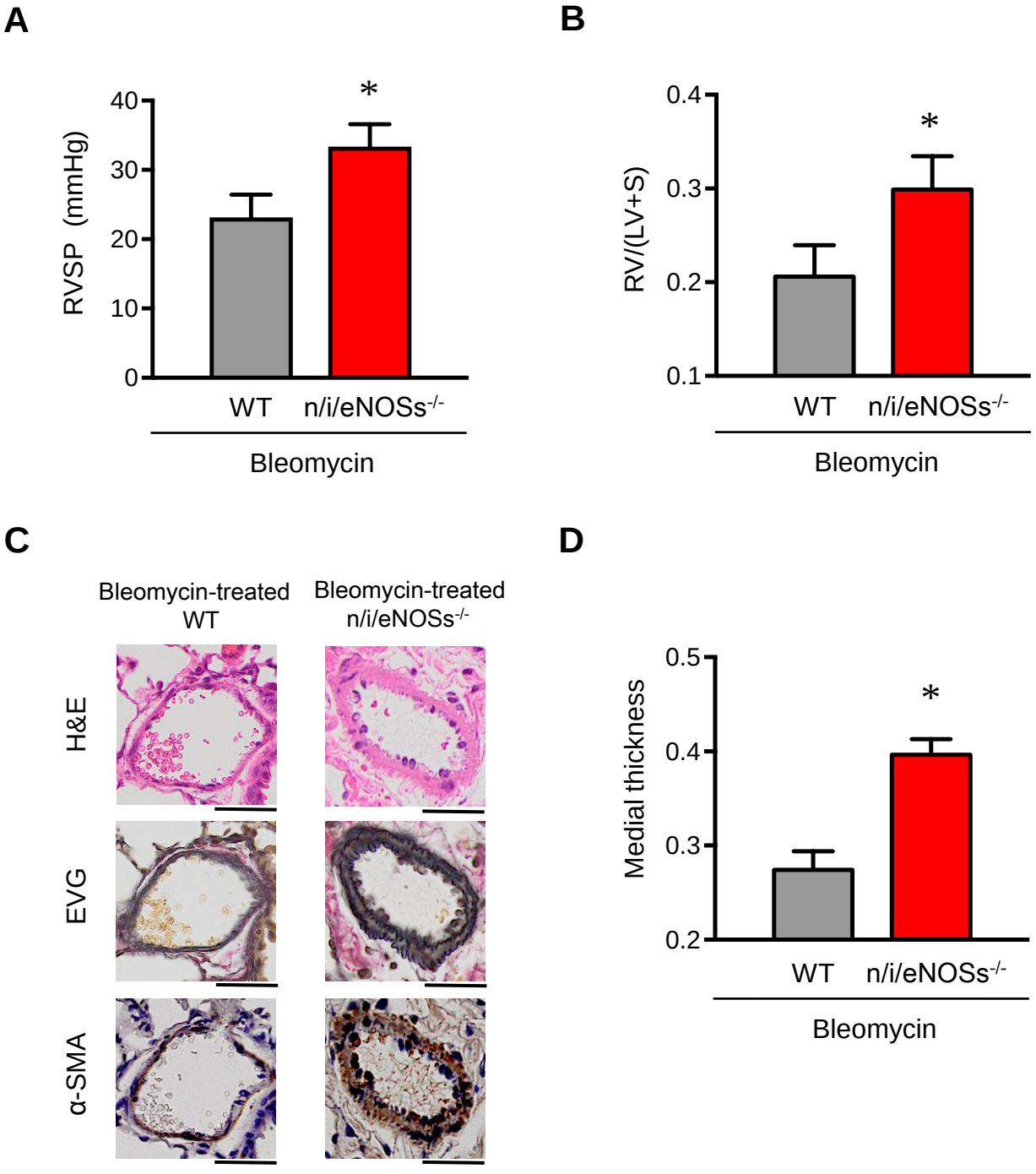

Supplementary Figure E6

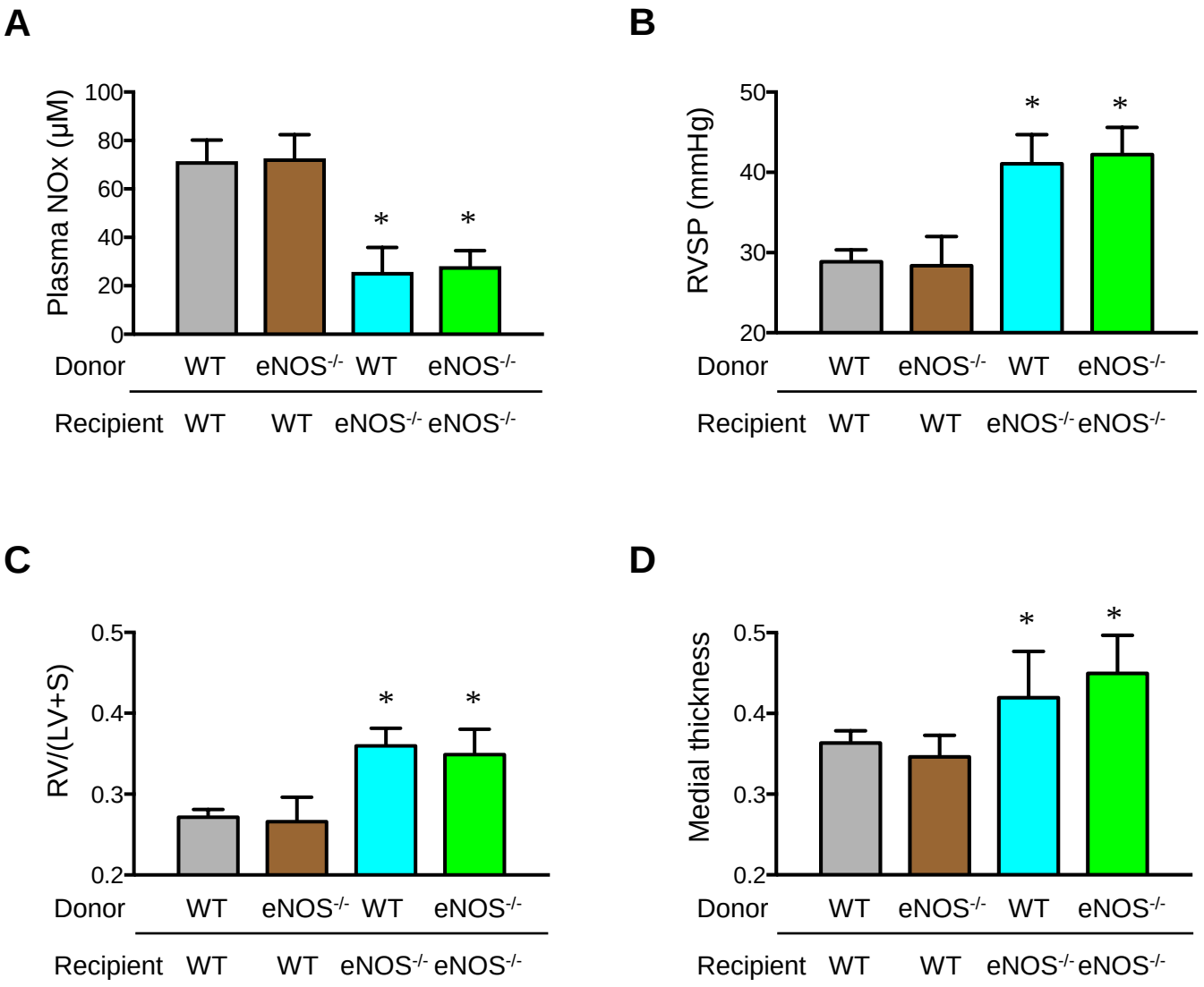

Supplementary Figure E7

AJRCCM Articles in Press. Published on 26-February-2018 as 10.1164/rccm.201709-1783OC

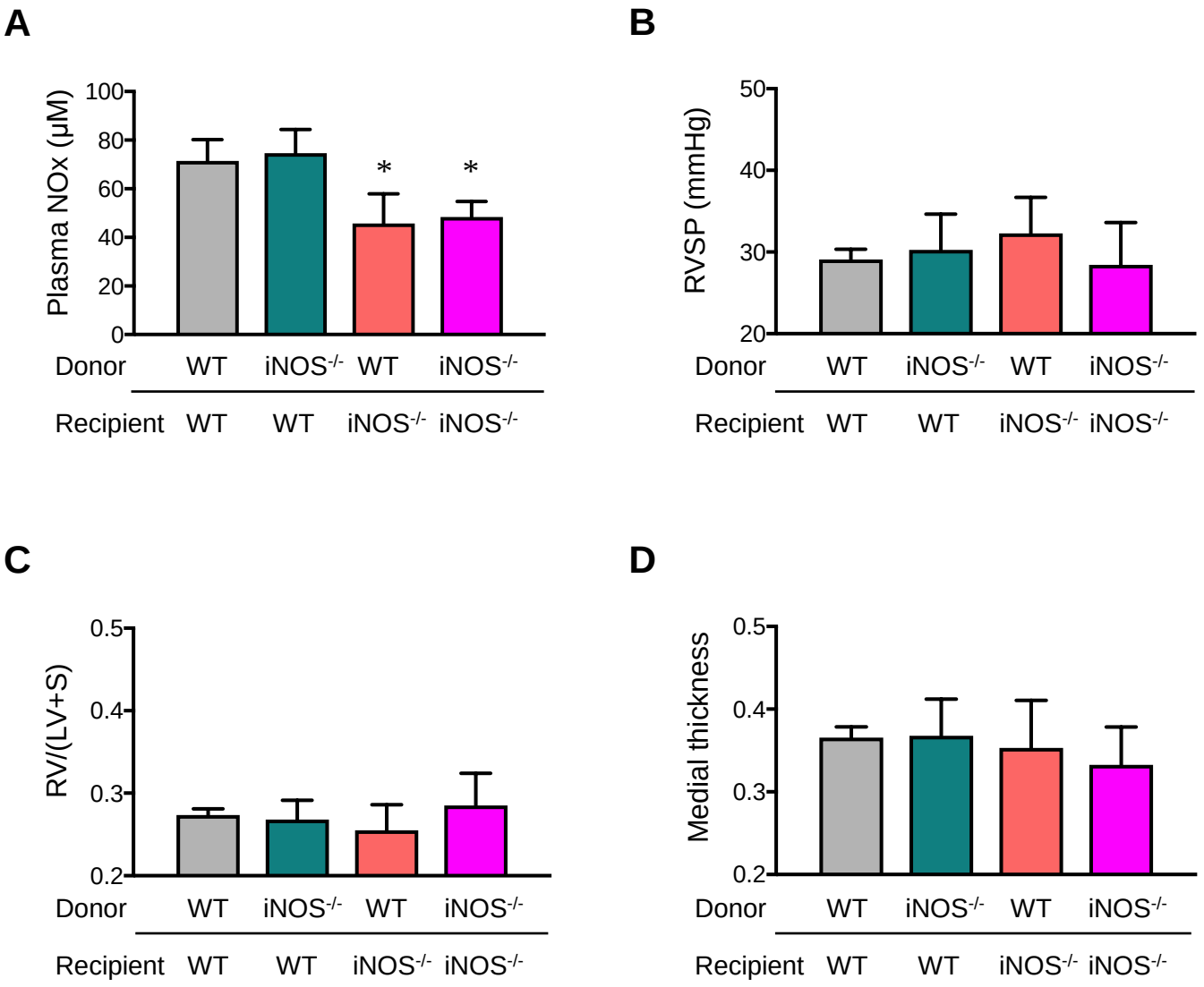

Supplementary Figure E8

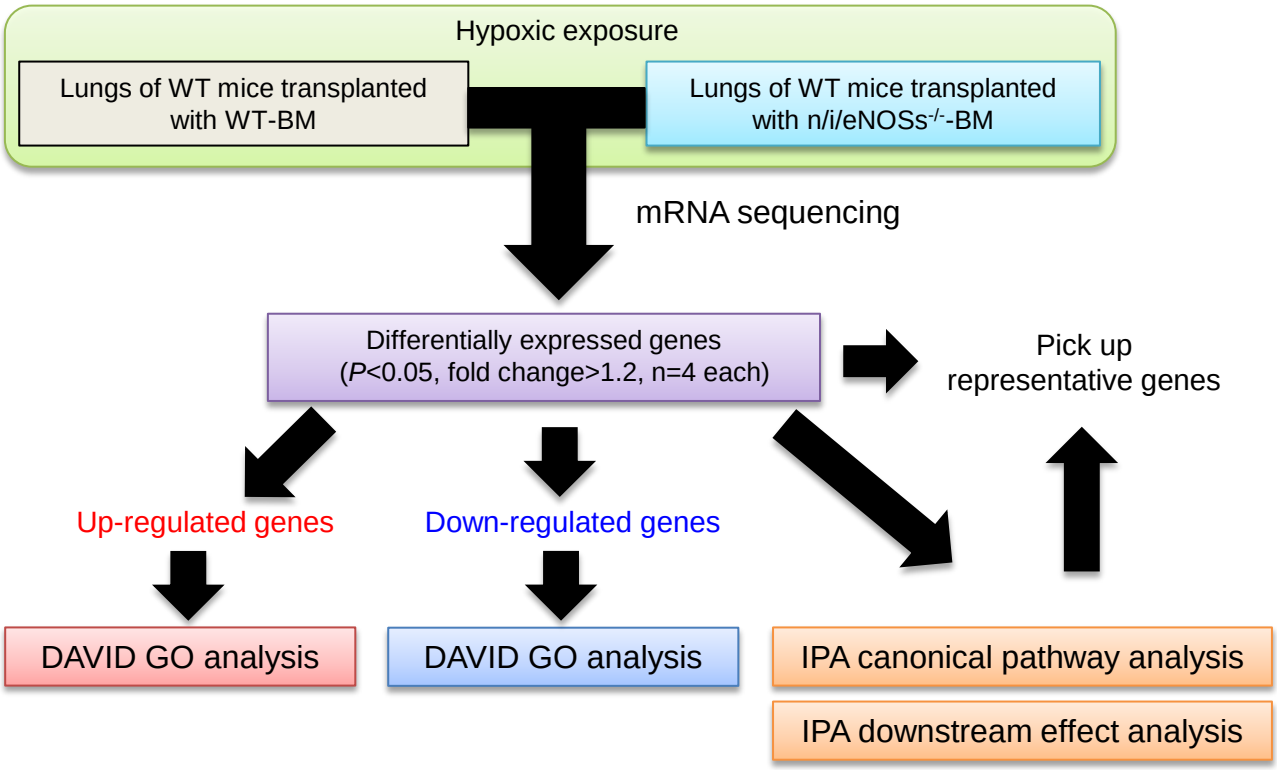

Supplementary Figure E9